

# Internal structure of basalt flows: insights from magnetic and crystallographic fabrics of the *La Palisse* volcanics, French Massif Central

T. Boiron,<sup>1,2</sup> J. Bascou,<sup>2</sup> P. Camps,<sup>3</sup> E. C. Ferré,<sup>4</sup> C. Maurice,<sup>1</sup> B. Guy,<sup>1</sup> M.-C. Gerbe<sup>2</sup> and P. Launeau<sup>5</sup>

<sup>1</sup>*Ecole nationale supérieure des mines de Saint Etienne, 158 cours Fauriel, 42023 Saint Etienne, France. E-mail: boiron@emse.fr*

<sup>2</sup>*Université de Lyon, UMR 6524, Magmas et Volcans, CNRS and Université Jean Monnet, 23, rue du Dr. Michelon, 42023 Saint Etienne, France.*

*E-mail: jerome.bascou@univ-st-etienne.fr*

<sup>3</sup>*Géosciences Montpellier, UMR 5246, CNRS and Université de Montpellier, 34095 Montpellier, France*

<sup>4</sup>*Department of Geology, Southern Illinois University, Carbondale, IL 62901–4324, USA*

<sup>5</sup>*Laboratoire de Planétologie et Géodynamique, UMR 6112, CNRS and Université de Nantes, 2 rue de la Houssinière, 44322 Nantes, France*

Accepted 2012 December 18. Received 2012 December 17; in original form 2011 December 20

## SUMMARY

We present a new interpretation of anisotropy of magnetic susceptibility (AMS) fabrics in basaltic lava flows based on the detailed study of magnetic mineralogy and silicate crystallographic fabric of a Quaternary lava flow from the French Massif Central (La Palisse). We consider the model of AMS fabric imbrication between magnetic foliation and flow surface, as initially proposed for dykes. At the two sampling sites, the concordance between the flow direction deduced from the AMS foliation and that deduced from field observations indicates that the imbrication model could apply to the lava flows. However, the flow senses inferred from AMS are systematically opposed between the two sampling sites suggesting permutations between  $K_1$  and  $K_3$  AMS axes, a configuration referred to as inverse fabric. Electron backscatter diffraction (EBSD) measurements show strong lattice-preferred orientations (LPO) for plagioclase, especially the (010) plagioclase plane, which tends to be parallel to the flow. Clinopyroxene LPO remains less marked than plagioclase LPO, whereas titanomagnetite does not display a significant LPO. Comparison between magnetic and crystallographic fabrics suggests that the AMS fabric of the lava flow results from the distribution of titanomagnetite grains, which is in turn controlled by the fabric of the silicate framework. Magnetic hysteresis parameters and anisotropy of remanent magnetization (ARM) measurements exclude a significant contribution from single-domain grains, often called upon to explain inverse magnetic fabrics. The origin of the observed inverse magnetic fabric may relate to the dip of the palaeosurface, which is the only remarkable difference between the two sampling sites. AMS appears as a good tool to determine the direction of basaltic lava flows and coupling with local crystallographic fabric data provides a valuable control of relationships between magnetic fabrics and flow and thus contributes to better constrain the AMS signature of lava flows.

**Key words:** Magnetic fabrics and anisotropy; Magnetic mineralogy and petrology; Rock and mineral magnetism; Microstructure; Effusive volcanism; Europe.

## 1 INTRODUCTION

The internal structure of basaltic lava flows may provide key information on flow mechanisms and on lava rheology (e.g. Ventura *et al.* 1996; Smith 2002). In general, macroscopic markers such as vesicles (e.g. Aubele *et al.* 1988) and measurement of lattice-preferred orientation (LPO) allow to investigate the internal structure of a flow (e.g. Long & Wood 1986; Smith 2002). However, the scarcity of

markers in these rocks which are weakly anisotropic and the time-intensive nature of LPO measurements are significant hindrances to systematic studies of a flow from bottom to top.

The main goal of this study is to investigate if the anisotropy of magnetic susceptibility (AMS) technique can provide reliable information on internal structures and flow direction. The AMS technique has already been successfully used elsewhere to track both magmatic and deformation fabrics on a wide variety of rocks

(e.g. Tarling & Hrouda 1993; Borradaile & Henry 1997; Bouchez 2000; Ferré *et al.* 2003; Borradaile & Jackson 2004), including volcanic rocks (e.g. Knight & Walker 1988; Cañón-Tapia 2004; Plenier *et al.* 2005; Loock *et al.* 2008; Petronis & Geissman 2009). The significance of magnetic fabrics in volcanic rocks has been questioned because these rocks tend to show a weak magnetic anisotropy, near the detection limit of the AMS technique (Tarling & Hrouda 1993).

Despite the weak anisotropy of the volcanic rocks, AMS measurements show relationships between magnetic fabric and flow: maximum susceptibility axis  $K_1$  tend to be parallel to the flow direction and minimum susceptibility axis  $K_3$  tend to be perpendicular to the flow plane (Cañón-Tapia *et al.* 1996, 1997; Herrero-Bervera *et al.* 2001; Zhu *et al.* 2003; Cañón-Tapia 2004; Raposo & Berquo 2008). However, complications have arisen regarding the significance of AMS fabrics and their relationship to magma flow directions (e.g. Rochette *et al.* 1999; Henry *et al.* 2003a; Plenier *et al.* 2005).

In dyke the imbrication model proposed by Knight & Walker (1988) considers that  $K_1$  and  $K_3$  should be oblique and symmetrical with respect to the flow direction and flow plane. In this case, the obliquity further indicates the flow sense. This model often uses  $K_1$  angle to determine the flow direction (Staudigel *et al.* 1992; Herrero-Bervera *et al.* 2001). When the magnitudes of  $K_1$  and  $K_2$  axes are too close (oblate magnetic fabrics), a switch occurs between these two axes. The flow direction can be determined using the distribution of  $K_3$  axes (Callot *et al.* 2001; Geoffroy *et al.* 2002). Callot & Guichet (2003) also proposed an analytical model in dykes and concluded that the determination of the flow direction with the maximum susceptibility axis is a misuse, and recommend generalizing the magnetic foliation use.

Complications could also occur when single-domain (SD) magnetite grains are significant contributors to AMS (Potter & Stephenson 1988). Indeed, in contrast to multidomain (MD) grains,  $K_1$  is parallel to the short axis and  $K_3$  is parallel to the long axis of SD grains. This generates an 'inverse' magnetic fabric (Rochette *et al.* 1999; Ferré 2002). Other difficulties to interpret the AMS signature could also appear due to magnetic interactions when the ferromagnetic (s.l.) grains are at close distance from each other (Grégoire *et al.* 1995; Fanjat *et al.* 2012), the effects of multiple mineral-preferred orientations (Hrouda 1992), viscous strain variations in magma (Dragoni *et al.* 1997), post-flow alteration (Park *et al.* 1988) or thermal contraction (Gil-Imaz *et al.* 2006).

In basaltic lava flows, AMS is also used to infer the flow direction (e.g. Cañón-Tapia *et al.* 1996, 1997; Bascou *et al.* 2005; Loock *et al.* 2008). The imbrication model is used to determine the flow direction with either  $K_1$  or  $K_3$ . In lava flows, inverse fabrics are also observed (Rochette *et al.* 1999). Other parameters as chemical composition related to viscosity or palaeosurface topography could influence the AMS fabrics (Cañón-Tapia *et al.* 1995; Merle 1998; Henry *et al.* 2003b). In addition, the identification of relationships between AMS and the flow direction may depend on height in the flow. In their AMS study from basaltic lava flow, Bascou *et al.* (2005) observe a stronger correlation between AMS and flow-related plagioclase-preferred orientation in the lower part of the lava flow than at other levels. Thus, the relationships between AMS and flow direction in a flow that could present variations from the base to the top in magnetic mineralogy, crystallographic and magnetic fabrics is still unclear.

In this study, AMS measurements were carried out on a Quaternary lava flow from the French Massif Central (La Palisse basaltic flow), which is exposed at different levels. A detailed study of the magnetic mineralogy has been performed and relationships between AMS and the flow related silicate framework were investigated

through 3-D crystallographic fabrics characterization of main minerals (plagioclase, clinopyroxene and titanomagnetite) using electron backscatter diffraction (EBSD).

## 2 GEOLOGICAL SETTINGS AND PETROLOGY

The La Palisse basaltic lava flow is located in the Bas-Vivarais volcanic province, in the East part of the French Massif Central (Fig. 1a). The volcanic activity of the Bas-Vivarais province is characterized by alternated phreatomagmatic eruptions and strombolian activity and is spread over a large time interval, from  $166 \pm 15$  to  $45.4 \pm 3.2$  ka (Guérin & Gillot 2007). The La Palisse lava flow belongs to an eruptive episode occurring around  $78.8 \pm 5.3$  ka (Guérin & Gillot 2007). Its emission source is at the Suc de Bauzon scoria cone, from which the flow went NW into the Loire palaeo-valley which was incised in the granitic substratum (Fig. 1b). The thickness of the flow is  $\approx 40$  m at the sampling sites.

Two sampling sites were selected to address distinct structural levels of the flow. In sampling site 1, the colonnade and the entablature are clearly observed. The apparent thickness of the colonnade ranges from less than 1 m to about 3 m. Columns are vertical, oriented perpendicularly to the horizontal substratum surface and have a mean width of 0.4 m. In the entablature level, in which thickness ranges from 6 to 12 m, columns are randomly oriented and only a few centimetres in width. In sampling site 2, three zones can be distinguished from base to top of (Fig. 2): the colonnade (from 1 to 3 m thick), an intermediate zone presenting planar layering and hereafter referred to as layered zone (from 1 to 2 m thick) and the pseudo-colonnade (from 2 to 4 m thick). The intermediate zone differs from the entablature level of site 1 by its planar structure. The strike of volcanic layers is NE–SW with a  $50^\circ$  dip to NW (Fig. 2). Because the La Palisse basalt flow is channelled by a palaeo-valley, the underlying palaeosurface, currently not outcropping, is assumed subhorizontal at site 1 and parallel to the layered zone at site 2.

Regardless of the structural level, the lava flow samples contain phenocrysts and xenocrysts of olivine, phenocrysts of clinopyroxene, microphenocrysts (50–500  $\mu\text{m}$  in size) of plagioclase and a groundmass mainly composed of microlites of plagioclase, clinopyroxene and iron oxides within partially devitrified glass. The fluidal texture displayed by plagioclase microphenocrysts is observed in the different levels of the two sampling sites, whereas the pseudo-colonnade level exhibits a more vesicular texture.

The La Palisse lava is basanite (from TAS diagram, Lebas *et al.* 1986). The mean composition of phenocrysts are An50 for plagioclase, Fo78 for olivine and diopside for clinopyroxene (Boiron 2011). The oxide grains are mainly Ti-rich titanomagnetite ( $\text{Fe}_{3-x}\text{Ti}_x\text{O}_4$  with  $x$  mean value of 0.6; Boiron 2011).

## 3 METHODS

### 3.1 Magnetic methods

The AMS was measured with a KLY-3 Kappabridge instrument (AGICO, Brno) at the University of Montpellier (France). Thermomagnetic experiments were mainly conducted under argon atmosphere, with a CS4 furnace coupled to a MFK1 Kappabridge instrument (AGICO, Brno) at the University of Saint Étienne (France). AMS in low-magnetic field ( $<1$  mT) is mathematically described as a symmetric second rank tensor, which can be geometrically expressed as an ellipsoid with three principal susceptibility axes

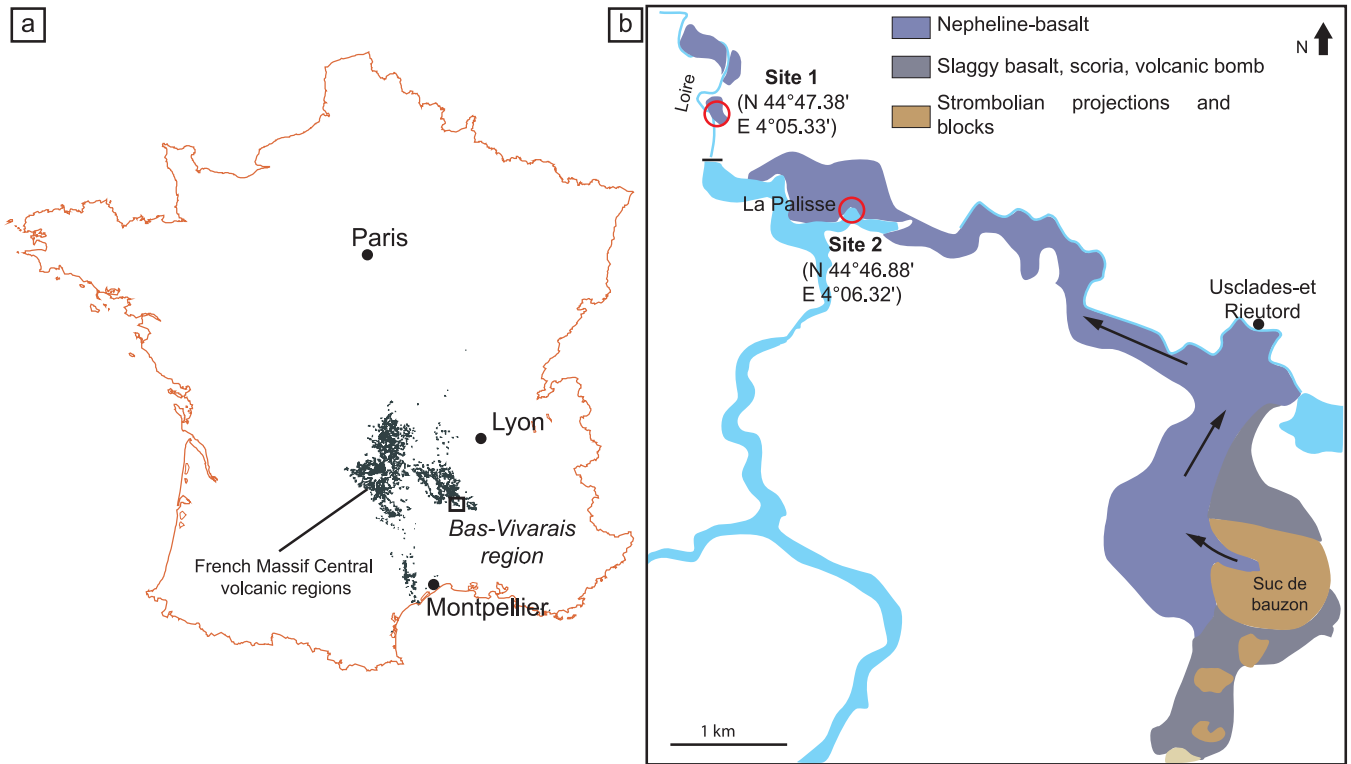


**Figure 1.** Location of the La Palisse basalt flow. (a) Location of the Bas-Vivarais volcanic region. Black area refers to the volcanic provinces of the French Massif Central, (b) Geological map of the studied area. Black arrows indicate the flow direction. The location of studied sites is also indicated. GPS data: Site 1: N 44°47.38', E 4°05.33', Site 2: N 44°46.88', E 4°06.32'.

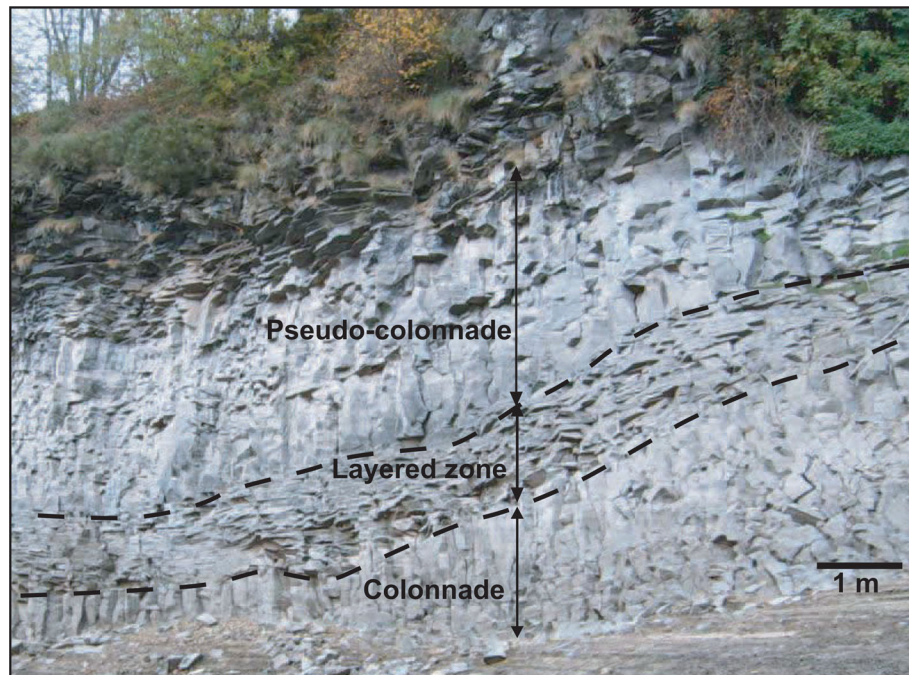


**Figure 2.** Photo of the La Palisse village outcrop (site 2) showing the colonnade, the layered zone and the pseudo-colonnade levels within the lava flow.

( $K_1$ ,  $K_2$  and  $K_3$  with  $K_1 \geq K_2 \geq K_3$ ). For magnetite, AMS is controlled by the shape-preferred orientation (SPO) of individual grains or aggregates (Rochette *et al.* 1992). Many parameters are usually employed to describe the AMS fabric of rocks. In this paper, we used the bulk magnetic susceptibility  $K_m = (K_1 + K_2 + K_3)/3$ , the corrected degree of anisotropy (Jelinek 1981).

$P' = \exp\sqrt{2[(\eta_1 - \eta_m)^2 + (\eta_2 - \eta_m)^2 + (\eta_3 - \eta_m)^2]}$ , where  $\eta_1 = \ln K_1$ ,  $\eta_2 = \ln K_2$ ,  $\eta_3 = \ln K_3$  and  $\eta_m = \eta = (\eta_1 + \eta_2 + \eta_3)/3$ , and the shape parameter (Jelinek 1981) defined as  $T = (2\eta_2 - \eta_1 - \eta_3)/(\eta_1 - \eta_3)$ . The  $P'$  parameter is used to quantify the degree of magnetic anisotropy and  $T$  characterizes the AMS ellipsoid shape.  $T$  ranges from  $-1$  (prolate shape) to  $+1$  (oblate



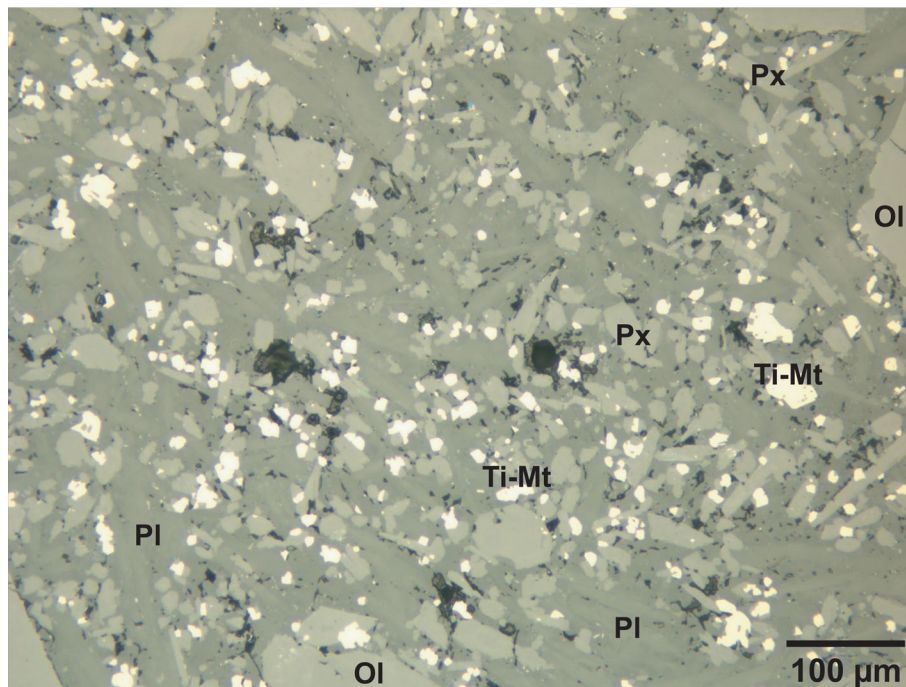


**Figure 3.** Reflected light photomicrograph of representative thin section from the colonnade of the La Palisse basalt flow (08tb14b sample; site 1). The white spots are mainly constituted of titanomagnetite grains (Ti-Mt). Pl, plagioclase; Px, pyroxene; Ol, olivine.

shape). Magnetic hysteresis and first order reversal curve (FORC) were measured on a Vibrating Sample Magnetometer Princeton Measurements 3900–04 at the University of South Illinois, Carbon-dale (USA). The anisotropy of anhysteretic remanent magnetization (A-ARM) measurements were carried out by three steps using a 2G cryogenic SQUID magnetometer with an alternating field (AF) demagnetizer at the University of Montpellier (France). The sample was first AF demagnetized along three perpendicular axes with a maximum magnetic field of 170 mT. In a second time, an ARM is acquired along a direction perpendicular to the last demagnetized axis with a bias direct field of 30  $\mu$ T and AF of 120 mT. In the third step, the induced ARM was measured. These three steps are repeated for six positions following the sequence,  $+X$ ,  $+Y$ ,  $+Z$ ,  $-X$ ,  $-Y$  and  $-Z$ .

### 3.2 LPO and SPO methods

The LPO of plagioclase, clinopyroxene and titanomagnetite was measured by indexation of electron-backscattered diffraction patterns (EBSD) with a Zeiss Supra 55 VP SEM at the École nationale supérieure des mines of Saint-Étienne (France). EBSD patterns are generated by interaction of a vertical incident electron beam with a carefully polished thin section tilted at  $70^\circ$ . The diffraction patterns are processed and indexed in terms of crystal orientation using the CHANNEL5 software from HKL, Oxford Instruments. Crystallographic orientations were measured grain-per-grain using an accelerating voltage of 20 kV, a working distance of 15 mm, a current intensity of 26  $\mu$ A and a pressure of 15 Pa. The diffraction images indexation was based on crystallographic data of respectively: Wechsler *et al.* (1984) for titanomagnetite, Wenk *et al.* (1980) for plagioclase and Bertolo *et al.* (1994) for clinopyroxene.

Image analysis was performed from sets of six digital photos on thin sections in polarized light with different angles (from  $0^\circ$  to  $150^\circ$ ) using a binocular microscope equipped with colour CCD in order to obtain images displaying a relatively wide surface of

analysis. The sets of digitized images were then processed and the SPO was calculated using the Intercept software developed by Launeau & Robin (1996). The 2-D SPO is represented by an ellipse characterized by the shape ratio ( $SR$  = ratio of the ellipse long/short axes) and the angle ( $\alpha$ ) between the ellipse long axis and the reference sample direction ( $X$ ). The 3-D SPO corresponds to the best ellipsoid calculated from the combination of ellipses taken on three perpendicular sections following the procedure of Launeau & Robin (2005) modified by Launeau *et al.* (2010); see also <http://www.sciences.univ-nantes.fr/lpgnantes/SPO>.

## 4 MAGNETIC MINERALOGY

The mode of titanomagnetite grains, determined by image analysis and reflected-light microscopy, is about 3 per cent in volume for each level in the flow (Fig. 3). Grains are subhedral in shape and exhibit a mean size around 15  $\mu$ m. The grains, observed through optical microscopy and SEM, appear free of exsolutions.

Thermomagnetic curves were performed on basaltic powder coming from sampling at different levels of the flow (Fig. 4). Curves are generally reversible and show a Curie temperature ( $T_C$ ) ranging from 100 to 140°C. These low  $T_C$  attest of the high titanium content of titanomagnetite, with an average composition of  $Fe_{2.4}Ti_{0.6}O_4$  (Dunlop & Özdemir 1997; Lattard *et al.* 2006). This composition is in agreement with microprobe data. Thermomagnetic analyses further suggest that the titanomagnetite grains are rather homogeneous in composition.

The hysteresis parameters were measured on 26 samples of the different levels from sites 1 and 2. Hysteresis curves clearly indicate the dominance of ferromagnetic (s.l.) minerals. The hysteresis curves are simple, no wasp-waisted shape being observed (Fig. 5a). The data in a plot of ( $M_{rs}/M_s$ ) versus ( $H_{cr}/H_c$ ) lies in the pseudo-SD (PSD) domain in agreement to data from other natural basaltic lava of similar composition with Ti-rich titanomagnetite (Fig. 5b;

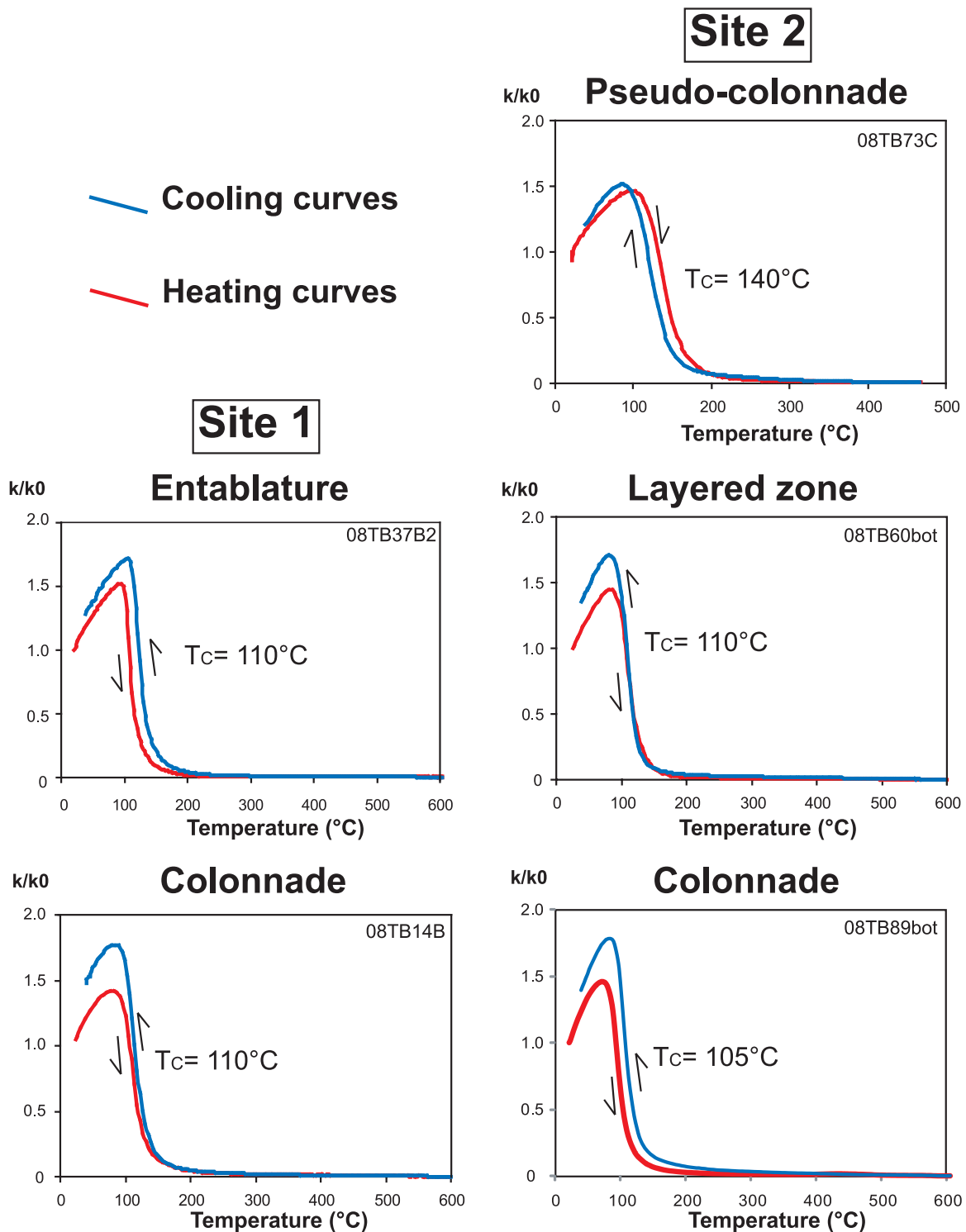


**Figure 4.** Magnetic susceptibility ( $K/K_0$ ) versus temperature for representative samples from the different levels of the La Palisse basalt for site 1 and 2. The thermomagnetic curves are commonly reversible and the rapid change in susceptibility indicates a Curie temperature ( $T_c$ ) of about  $110^\circ\text{C}$  associated to the Ti-rich titanomagnetite grains. Thermomagnetic curves determination under argon atmosphere at heating rate of  $11^\circ\text{C min}^{-1}$ .

Hartstra 1982; O'Donovan *et al.* 1986). According to Dunlop (2002), the PSD grain size range is narrower for Ti-rich titanomagnetite than for magnetite and could extend from approximately 2–25  $\mu\text{m}$ . The observed hysteresis properties are ambiguous and could result from either an intermediate and homogeneous grain size between SD and MD grains, or from a mixture of various SD

and MD grain sizes. In order to precise the potential contribution of SD grains, first order reveal curves (FORC) diagrams were carried out on samples from site 1 and 2. FORCs are expressed by contour plots of a 2-D distribution function and they provide an accurate mean to reveal information on the different components in a mixed magnetic mineral assemblage (Pike *et al.* 1999; Roberts

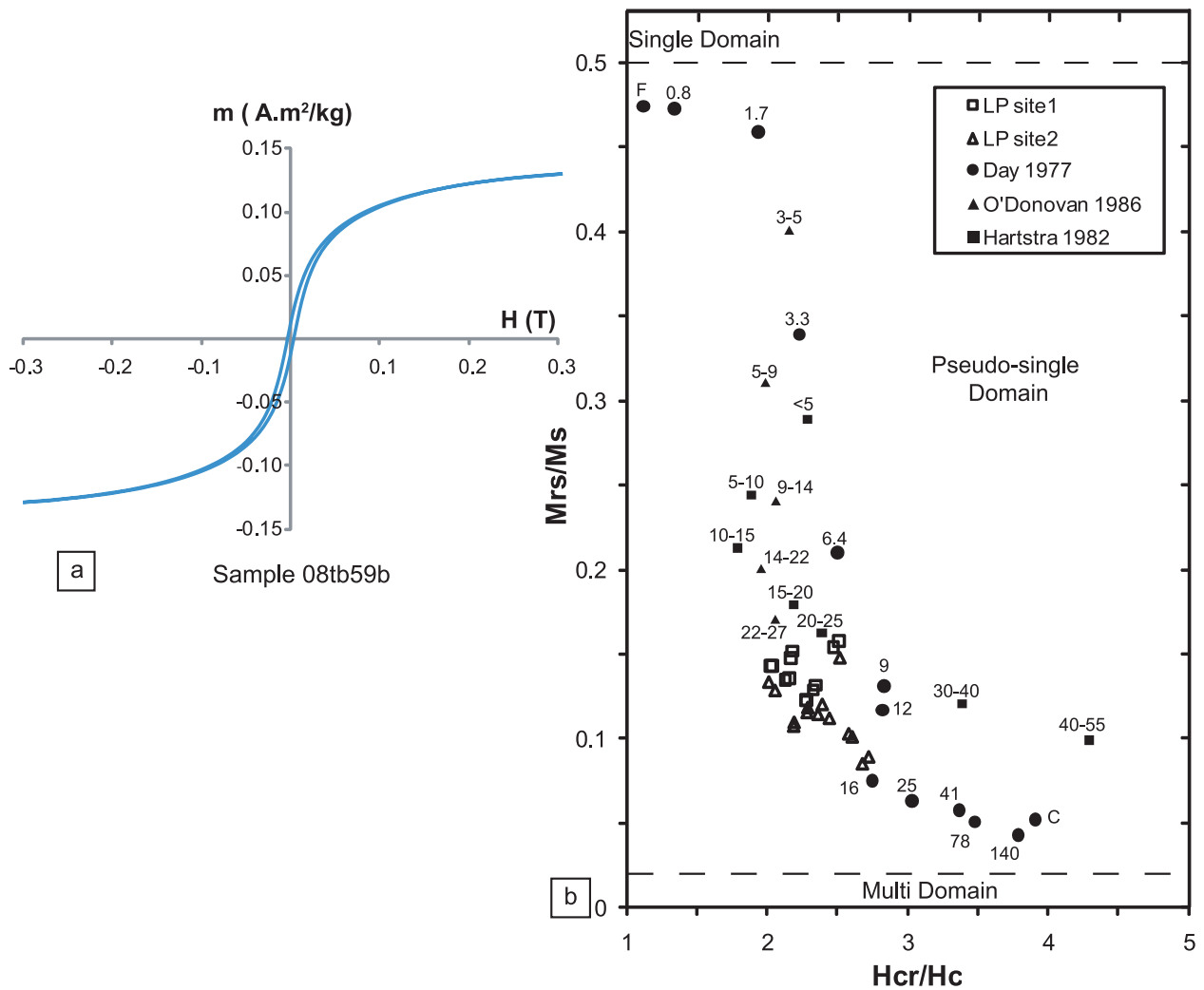


**Figure 5.** (a) Representative hysteresis curves (magnetic moment,  $m$  versus applied field,  $H$ ) indicating the presence of ferromagnetic (s.l.) grains. (b)  $M_{rs}/M_s$  ratio versus  $H_{cr}/H_c$  ratio diagrams of samples from the different levels of site 1 (LP site 1) and site 2 (LP site 2).  $M_{rs}$ , saturation remanence;  $M_s$ , saturation magnetization;  $H_{cr}$ , remanent coercive force;  $H_c$ , ordinary coercive force. The limits of the pseudo-single domain of titanomagnetite (TM60) are defined from Dunlop (2002). Titanomagnetite experimental data are reported from Day *et al.* (1977). Titanomagnetite grains belong to the pseudo-single domain (PSD) are consistent with data, also reported, from natural Ti-rich titanomagnetites (Hartstra *et al.* 1982; O'Donovan *et al.* 1986). Numbers indicate the grain size in micrometers, C (coarse grain) and F (fine grain) for experimental data.

*et al.* 2000). FORC diagrams obtained from four samples from the colonnade (08tb12 and 08tb18, site 1) and from the layered zone (08tb59 and 08tb68, site 2) are provided on Fig. 6. The outer contours diverge from the  $H_u = 0$  axis and intersect the  $H_c = 0$  axis whereas the inner contours are less divergent. The absence of any central peak in the four FORC diagrams confirms a very small contribution of SD particles (Roberts *et al.* 2000) and suggests a dominating PSD + MD mixing in the samples.

## 5 AMS

### 5.1 AMS scalar parameters

For site 1, the anisotropy degree  $P'$  is higher in the entablature level ( $P'$  mainly ranges from 1.03 to 1.11) than in the colonnade level ( $P'$  mainly ranges from 1.01 to 1.08) whereas the mean susceptibility  $K_m$  is lower in the entablature ( $K_m$  mainly ranges from  $4.1 \times 10^{-2}$  SI to  $5.3 \times 10^{-2}$  SI) than in the colonnade ( $K_m$  mainly ranges from

$4.9 \times 10^{-2}$  SI to  $5.8 \times 10^{-2}$  SI; Fig. 7a). In the entablature level, the distribution of the shape parameter ranges around a value of  $T = 0$  (triaxial shape). On the other hand, the shape parameter is more scattered in the colonnade (Fig. 7b). For site 2, the range of  $P'$  values of the pseudo-colonnade is narrower (around 1.03) than for colonnade and layered zone, from 1.02 to 1.06 and from 1.01 and 1.08, respectively. The mean susceptibility  $K_m$  is similar for the colonnade and the layered zone ( $5.0 \times 10^{-2}$  SI  $< K_m < 6.1 \times 10^{-2}$  SI) whereas it is lower in the pseudo-colonnade ( $4.3 \times 10^{-2}$  SI  $< K_m < 5.0 \times 10^{-2}$  SI; Fig. 7c). The shape parameter  $T$  for the layered zone and the colonnade is scattered in oblate and prolate domains with a larger number of data for the oblate shape. Pseudo-colonnade mainly spans the oblate domain ( $0.2 < T < 0.7$ ; Fig. 7d).

### 5.2 AMS fabrics

AMS fabrics measured in the different flow levels of sites 1 and 2 are presented on stereograms in the geographic referential (Fig. 8).

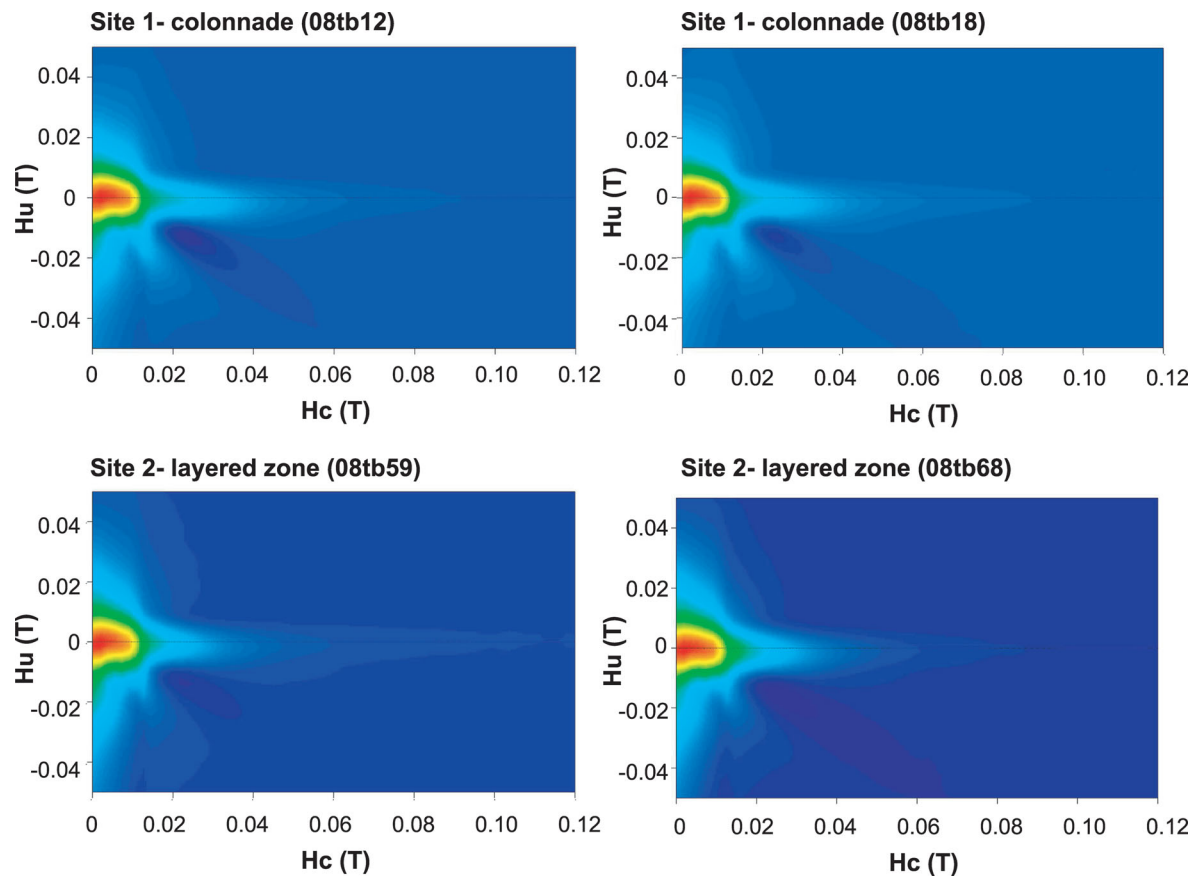


**Figure 6.** FORCs diagrams from site 1 colonnade (samples 08tb12 and 08tb18) and from site 2 layered zone (samples 08tb59 and 08tb68). These diagrams are characteristic of pseudo-single domain + multidomain grains mixing.

In all stereograms, the AMS eigenvectors ( $K_1 \geq K_2 \geq K_3$ ) are well grouped with narrow confidence ellipse and therefore the mean of principal susceptibility axes is statistically significant. The  $K_3$  axes for site 1 are particularly well grouped and the mean  $K_3$  displays close strike and dip. Maximum and intermediate axes are also well grouped but seem to be inverted between the colonnade and the entablature. For site 2, the minimum susceptibility axes remain the most grouped for all levels. The orientation of the mean principal susceptibility axes ( $K_1, K_2, K_3$ ) is similar in the colonnade and the layered zone but different for the pseudo-colonnade.

The determination of flow direction and flow sense from AMS fabrics is obtained by means of the imbrication of the magnetic foliation with a subhorizontal palaeosurface for site 1. For site 2, the palaeosurface is assumed to be parallel to the layered zone (NE–SW striking and  $50^\circ$  NW dipping; Fig. 8). The flow direction is given by the pole of the palaeosurface plane and the pole of magnetic foliation (i.e. the minimum principal axis  $K_3$ ). The angle between  $K_3$  and the palaeosurface defines the imbrication angle that allows determining the flow sense (Geoffroy *et al.* 2002). For site 1, flow direction and flow sense deduced from AMS are consistent with field observations, both for the colonnade and the entablature. Similarly, for site 2 a good correlation between flow direction deduced from AMS for the colonnade and the layered zone and from field observations is obtained. For the pseudo-colonnade, the  $K_3$  direction at high angle ( $>50^\circ$ ) perpendicularly to the layered plane, in comparison to the lower levels suggests an opposite imbrication located on the top of the flow. However, the magnetic foliation for pseudo-colonnade is strongly tilted and the imbrication angle is less clear for this level.

In addition, it must be noted that the flow sense deduced from AMS for the colonnade and the layered zone is opposed to field observations. The expected AMS diagram for site 2 with respect to the field geological evidences and the coherent AMS measurements for site 1, suggest an inversion between the maximum and the minimum axis for the colonnade and the layered zone of site 2.

## 6 MAGNETIC AND CRYSTALLOGRAPHIC FABRICS

### 6.1 LPO

The LPO of plagioclase, clinopyroxene and titanomagnetite are presented on equal area and lower hemisphere projections in the specimen reference framework for the colonnade and the entablature of site 1 (Fig. 9a) and for the colonnade, the layered zone and the pseudo-colonnade of site 2 (Figs 9b and c). Density contours are expressed in multiple uniform distribution (MUD) using the software PFch5 developed by David Mainprice (ftp://www.gm.univmontp2.fr/mainprice//CareWare\_Unicef\_Programs/, University of Montpellier, France). The fabric strength is expressed by the texture index  $J$  (Bunge 1982), which ranges from 1 in the case of random orientation to  $\infty$  in the case of an ideal single crystal.

Plagioclase presents the highest fabric strength ( $4.5 < J < 5.8$ ). The plagioclase (010) plane systematically shows the strongest maximum of density. For site 1, (010) maximum of density values of plagioclase from the colonnade and the entablature are 4.40 and

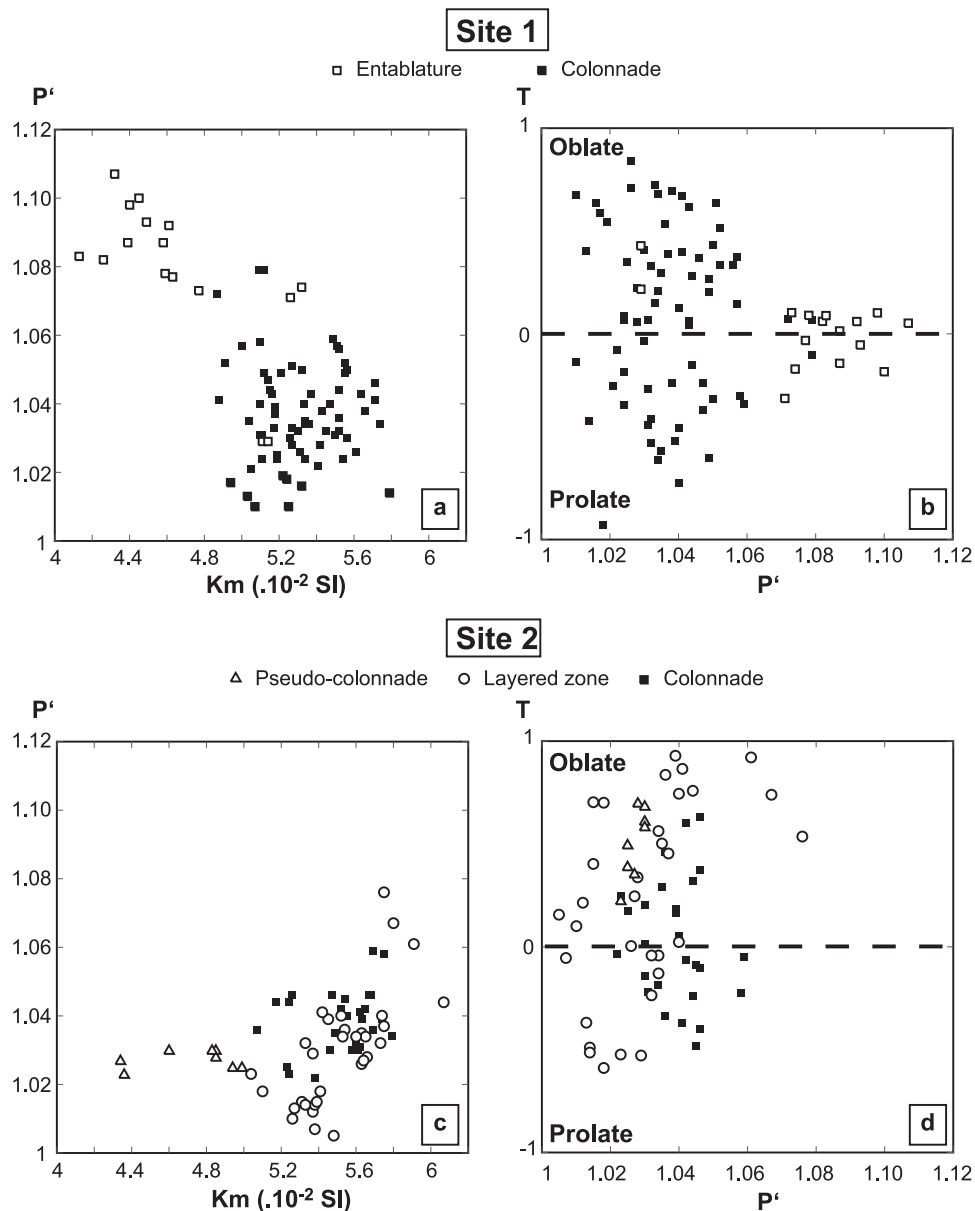


**Figure 7.** Diagrams representing the anisotropy parameter  $P'$  versus the bulk magnetic susceptibility ( $K_m$ ) for the different levels of site 1 (a) and site 2 (c). Diagrams of  $P'$  versus the shape parameter  $T$  are shown in (b) and (d) for site 1 and site 2, respectively.

5.37, respectively. Lower maximum of density values are observed for (100) plagioclase (3.68 and 4.38) and (001) plagioclase (2.24 and 2.81). For site 2, maximum of density values of (010) plagioclase for the colonnade, the layered zone and the pseudo-colonnade are 4.91, 5.23 and 4.81, respectively, while lowest value are observed for the (100) and (001) plagioclase. The highest (010) plagioclase maximum of density values are reached for the entablature of site 1 and for the layered zone of site 2. The highest values of the plagioclase fabric strength  $J$  are also reached in these zones (5.5 in the site 1 entablature and 5.8 in the site 2 layered zone). However, the site 2 colonnade and pseudo-colonnade present high fabric strengths as well ( $J > 5$ ).

Clinopyroxene LPO is not as strong as plagioclase LPO with a fabric strength  $J$  that ranges from 3.35 to 3.70. Maximum of density values are generally lower than 3 except for the entablature and the layered zone for which the (001) plane is higher (3.73 and 3.63, respectively).

Close relationships are observed between crystallographic planes of plagioclase and clinopyroxene: (100) plagioclase tends to be parallel to (001) clinopyroxene and (010) plagioclase tends to be parallel to (100) clinopyroxene for the two sites and at all levels.

Finally, no clear preferred orientation can be deduced from the LPO of titanomagnetite, even considering maximum of density values higher than 2. However, it can be noticed that (100) titanomagnetite has the highest maximum of density compared to (111) and (110) titanomagnetite, especially for the colonnade at both site 1 and 2 (maximum of density values of 2.30 and 2.49, respectively).

## 6.2 Comparison between magnetic and crystallographic fabrics

In order to precise the relationships between the plagioclase crystallographic-preferred orientations and the AMS, we compared the orientation of  $K_1$ ,  $K_2$  and  $K_3$  axes with the plagioclase



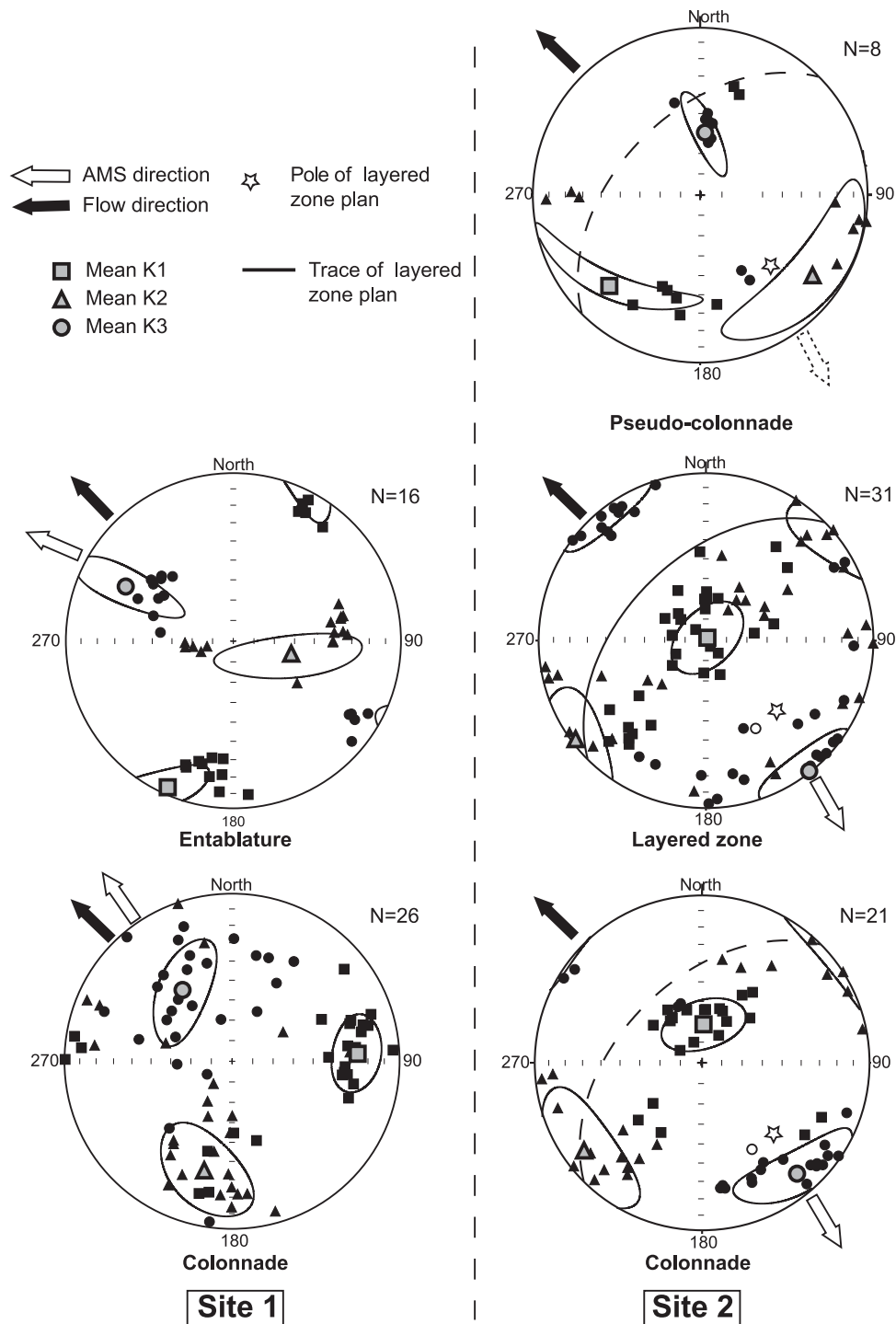


**Figure 8.** Equal area projection in the lower hemisphere and geographical referential of the principal magnetic susceptibilities axes ( $K_1$ ,  $K_2$ ,  $K_3$ ) measured in specimens from the different levels of the La Palisse flow for sites 1 and 2. The flow direction inferred from field observations is shown by the black arrow and the flow direction determined from AMS study is shown by the white arrow. The confidence ellipses are computed from Jelinek's statistics (Jelinek 1978).  $N$  is the number of measurements. For site 2, the layered flow plane is also presented in full line for layered zone and in dashed line for colonnade and pseudo-colonnade.

crystallographic fabrics on samples representative of the different flow levels. The principal susceptibility axes, as well as the best axes (eigenvectors) and the maximum of density of (100), (010) and (001) plagioclase were projected on lower hemisphere stereograms

in the specimen referential (Fig. 10). For site 1, in both colonnade and entablature levels, a clear correlation appears between the maximum susceptibility  $K_1$  and the 'Best Axis' of (100) plagioclase, between the minimum susceptibility  $K_3$  and the 'Best Axis' of (010)

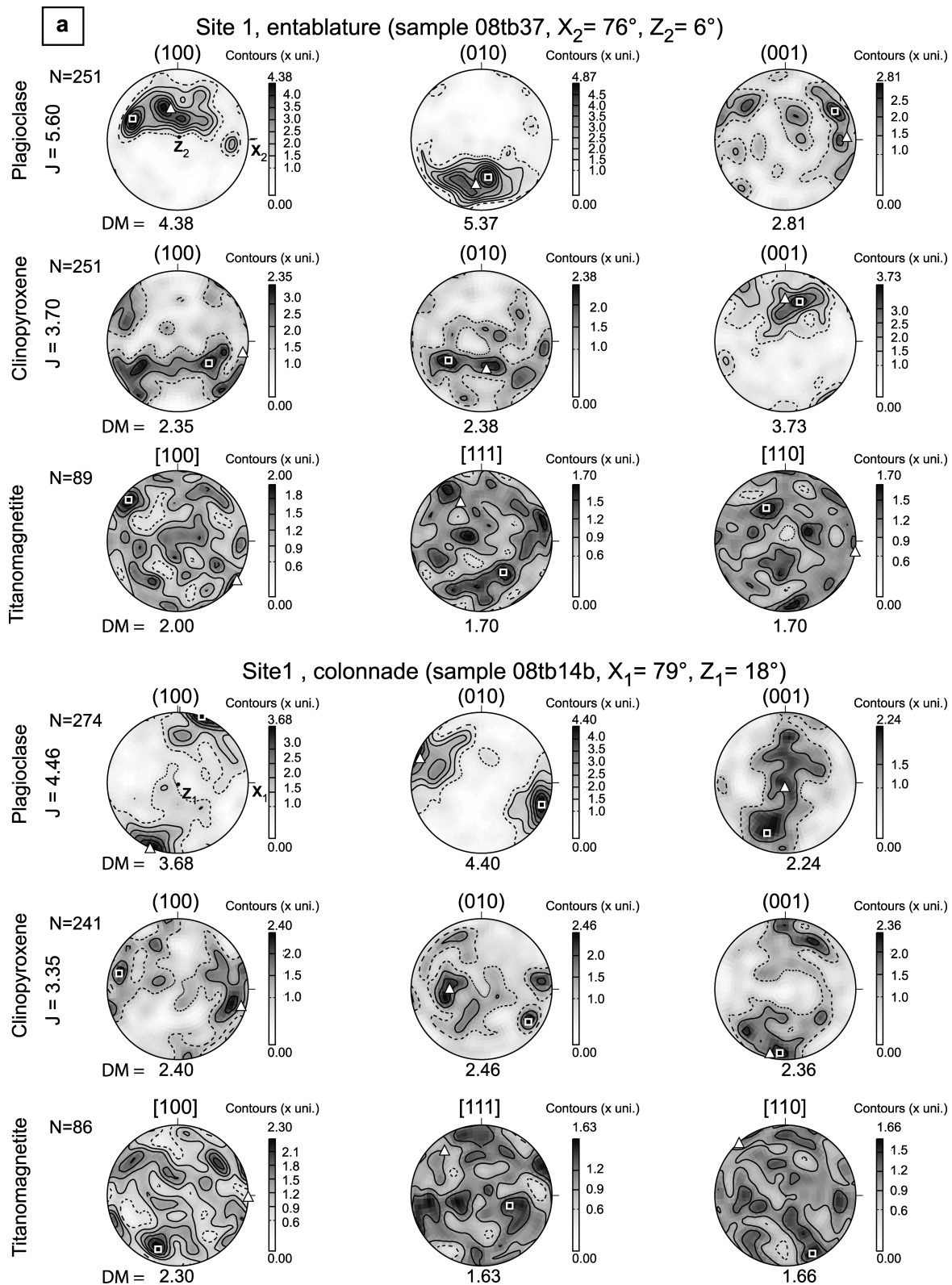


**Figure 9.** Lattice-preferred orientation (LPO) of plagioclase, clinopyroxene and titanomagnetite of samples from the different levels of the La Palisse flow: (a) from the colonnade and the entablature of site 1, (b) from the colonnade and the layered zone of site 2 and (c) from the pseudo-colonnade of site 2. Equal area, lower hemisphere projection in the specimen coordinates system with the field measured sample angles  $X$  (azimuth) and  $Z$  (dip). Contours are in multiples of uniform distribution (MUD).  $DM$  is the maximum of density, (black square in pole figures); white triangle represents the 'Best Axis';  $J$  is the texture index;  $N$  is the number of measurements. (d) Representative habitus of plagioclase, clinopyroxene and titanomagnetite single crystals.

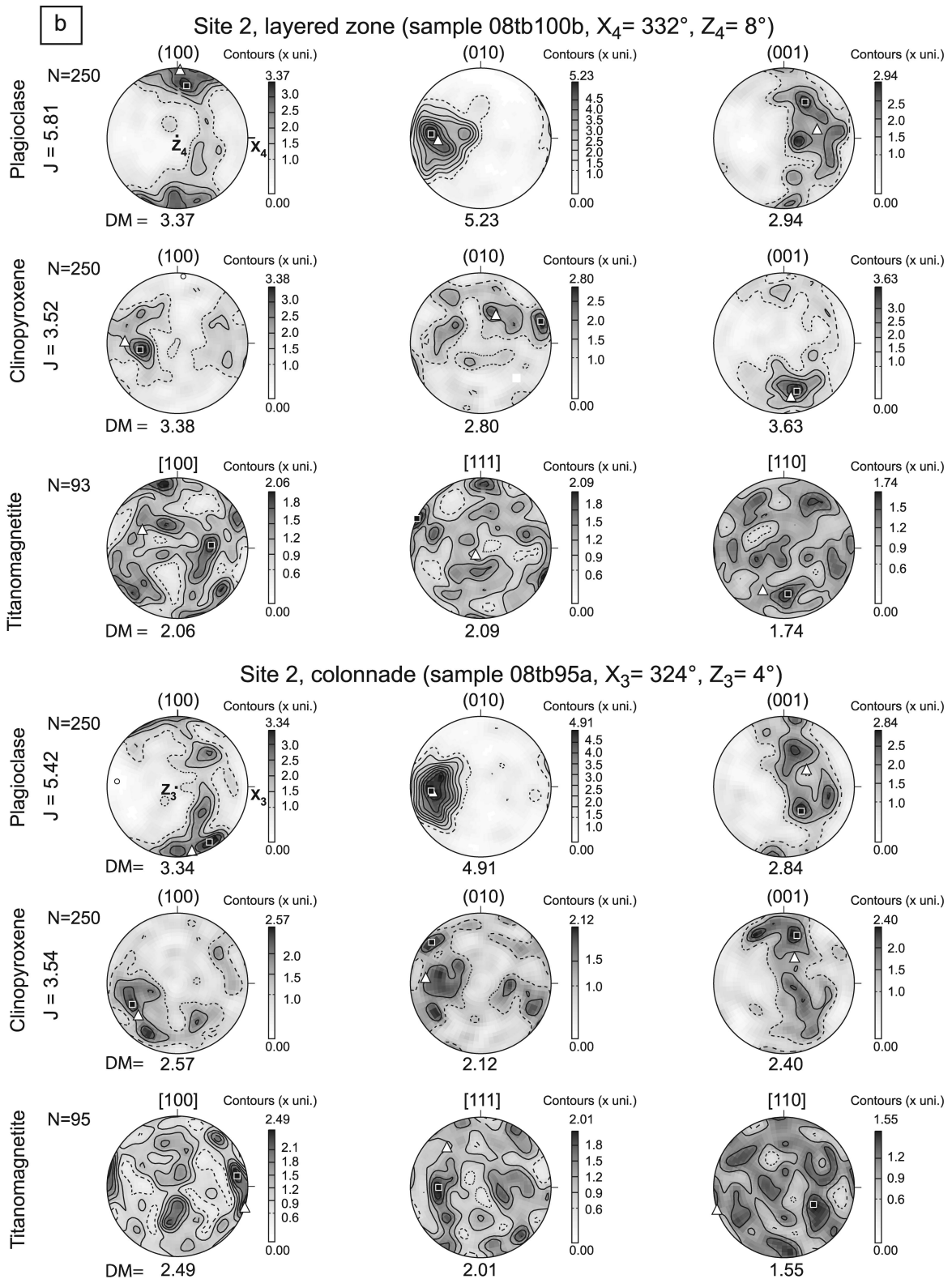


Figure 9. (Continued.)

plagioclase and between the intermediate susceptibility  $K_2$  and the 'Best Axis' of (001) plagioclase. For site 2, relationships are less obvious: (100) plagioclase is related to  $K_3$  in the pseudo-colonnade, but related to  $K_2$  in the layered zone and (001) plagioclase presents

a clear correlation with  $K_2$  in the pseudo-colonnade and also with  $K_3$  (DM Pl) in the colonnade. The (010) plagioclase 'Best Axis' shows high orientation correlations with  $K_1$  in the three flow levels.

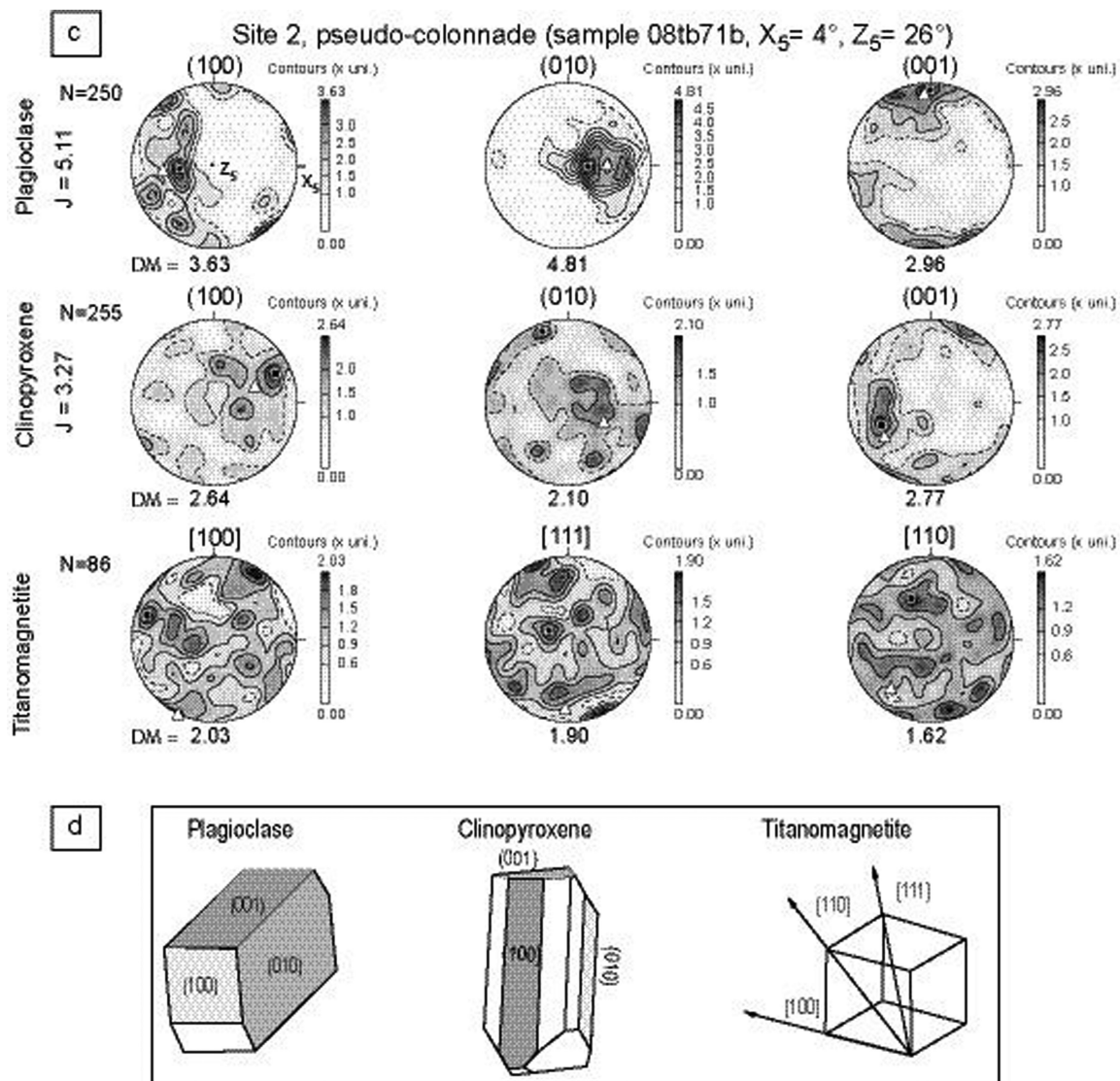


Figure 9. (Continued.)

## 7 DISCUSSION

### 7.1 Relation between AMS and flow

The results of this study show that the use of AMS to determine the flow direction, which is largely employed in dykes (e.g. Knight & Walker 1988; Geoffroy *et al.* 2002; Hastie *et al.* 2011), is also efficient in lava flows. We can notice that neither the maximum of magnetic susceptibility axis itself nor the imbrication of the magnetic lineation allow to find a flow direction that fit with the flow direction deduced from field evidences. In accord with previous AMS studies of lava flows (Saint-Thibéry; Bascou *et al.* 2005), the magnetic foliation imbrication appears as the best mean to obtain an accurate flow direction. Concerning the flow sense, our results are contrasted. For site 1, the flow sense deduced from AMS coincides with the field observations, whereas for site 2, they are systematically opposed. The flow sense deduced from AMS for site 2 appears to coincide with a permutation between the minimum and the maximum axes compared to site 1. The origin of the inversion of AMS axes is discussed in a following part.

### 7.2 Origin of AMS

Magnetic anisotropy of volcanic rocks can result from different intrinsic properties of minerals such as: magnetocrystalline anisotropy, shape anisotropy and a nonintrinsic property as the distribution anisotropy that could result from clustering of small and equant ferromagnetic grains (Hargraves *et al.* 1991). Petrographical observations indicate that the titanomagnetite grains, which are the main carrier of the AMS in the La Palisse basalt flow, are subhedral. As a consequence, shape anisotropy of individual grains can be neglected. In addition, titanomagnetite LPO is randomly oriented that excludes a magnetocrystalline anisotropy, in particular a preferred orientation of (100) titanomagnetite that corresponds to the best magnetization axis (Dunlop & Özdemir 1997). For lava flow, experimental studies of Hargraves *et al.* (1991) indicate that AMS can be produced from an anisotropy distribution of ferromagnetic particles constrained by a silicate 'template'.

Image analysis based on 2-D and 3-D images was performed in order to precise the relationships between crystallographic and magnetic fabrics. The shape ellipse from image analysis is shown



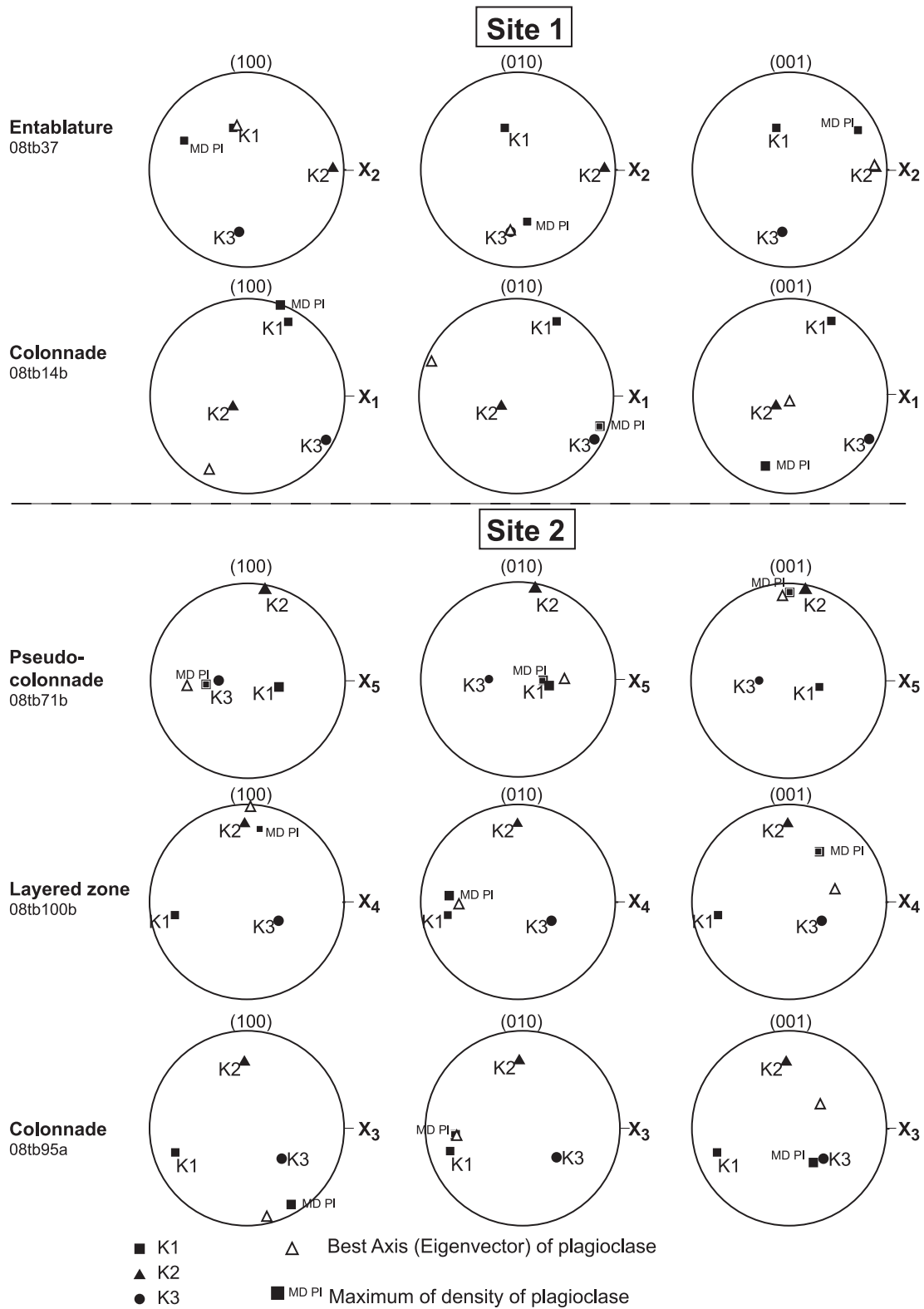


**Figure 10.** Projection in the specimen referential (as Fig. 9) of maximum of density (DM-PI) and ‘Best Axis’ (eigenvector) of plagioclase LPO for samples from the different flow levels. Maximum of density of titanomagnetite (111) axes and mean eigenvectors  $K_1$ ,  $K_2$  and  $K_3$  are plotted.

for site 1 (colonnade) where AMS signature is coherent with field flow direction and sense and for site 2 (pseudo-colonnade) where an inversion between  $K_1$  and  $K_3$  is observed relative to their plagioclase relationship in site 1 (Fig. 11).

For site 1, magnetic fabric, SPO and LPO of plagioclase show close relationships. The ‘magnetic lineation’ ( $K_1$ ) is parallel to plagioclase (100) ‘Best Axis’ and also parallel to the lath of plagioclase alignment. The “magnetic foliation” (plane perpendicular to  $K_3$ ) is

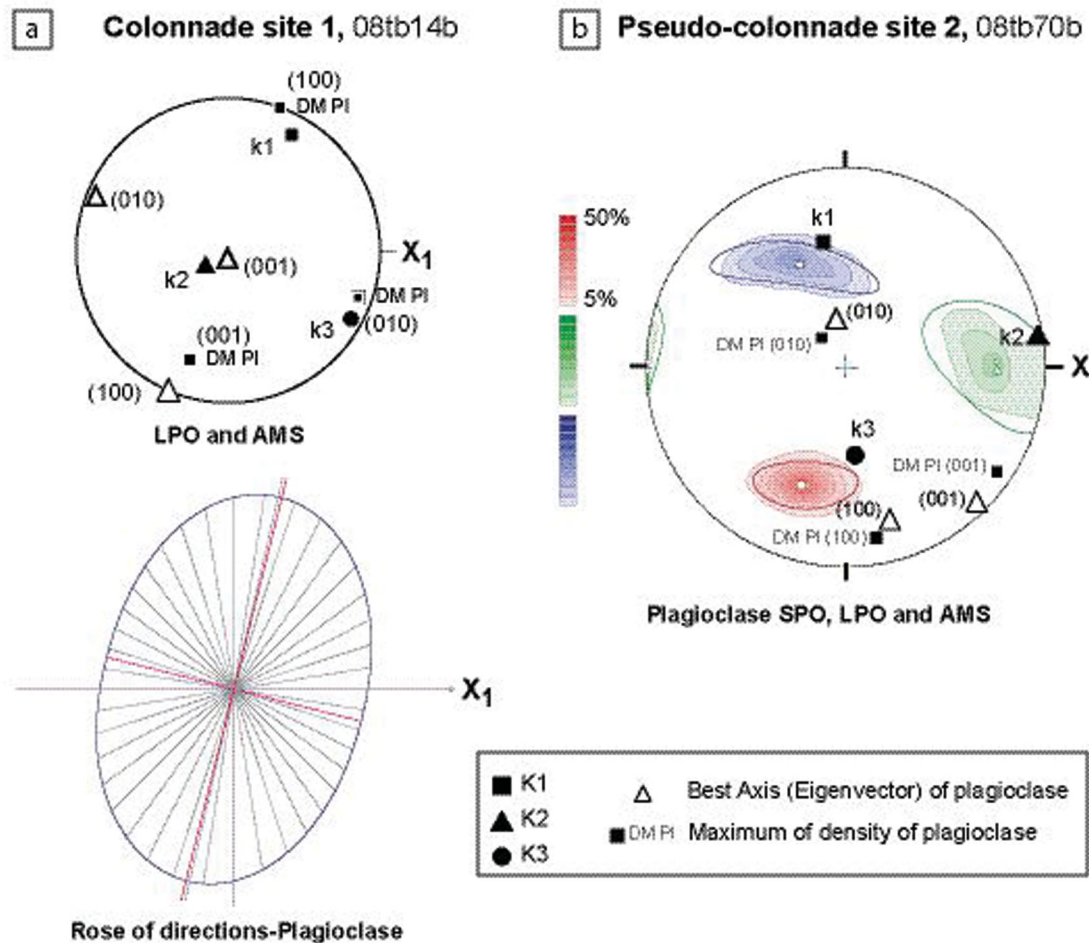


**Figure 11.** (a) Projection of plagioclase LPO [maximum of density (DM-PI) and 'Best Axis'] and AMS fabrics in lower hemisphere and specimen referential of 08tb14b sample from the colonnade site 1, compared to the shape-preferred orientation (SPO) of plagioclase deduced from 2-D image analysis (rose of mean length intercepts);  $SR = 1.468$ ,  $\alpha = 76^\circ$ . (b) Projection of plagioclase LPO, AMS and 3-D plagioclase SPO of 08tb70b sample from the pseudo-colonnade site 2.

parallel to plagioclase (010) and corresponds to the flow plane (Fig. 11a). These relationships between magnetic and the related flow crystallographic-preferred orientation of plagioclase are totally coherent with the crystal habitus 'in lath' of plagioclase. The tight relationships between the crystallographic (LPO and SPO) and magnetic fabrics strongly suggest that plagioclase laths mainly control the spatial distribution of titanomagnetite grains, carrier of the AMS. In addition, EBSD analyses show that clinopyroxene and plagioclase LPO are coaxial and therefore, both flow related. Plagioclase and clinopyroxene could constitute a silicate framework that constrains the spatial distribution of titanomagnetite grains. These results are in accordance with the experimental studies of Hargraves *et al.* (1991) and observations in natural flow by Bascou *et al.* (2005).

For site 2, magnetic and crystallographic fabrics are also coaxial. However, contrary to site 1, relationships between AMS and crystallographic axes differ between the different levels, except for  $K_1$  that systematically coincide to the (010) plagioclase 'Best Axis' (Fig. 10). In the pseudo-colonnade (site 2), the relationship between crystallographic and magnetic fabric shows a permutation of  $K_1$  with  $K_3$  compared to those observed for site 1. The (100) plagioclase 'Best Axis' tends to be parallel to  $K_3$  and to the long axis of the shape fabric (SPO) and the (010) plagioclase 'Best Axis' tends to be parallel to  $K_1$  and the short axis of the shape fabric (Fig. 11b).

### 7.3 Inverse AMS fabrics of La Palisse flow

Distinctive AMS fabrics from those measured for site 1, which are considered normal because of their agreement with field observations and relationships with plagioclase (and clinopyroxene) crystallographic fabrics, are observed in the different levels of site 2. For the colonnade and the layered zone of site 2, a systematic permutation of  $K_1$  and  $K_3$  axes could allow to define a flow sense conform to the field evidences. Such inversion between  $K_1$  and  $K_3$  is defined as an inverse magnetic fabric. Such fabric has already been described in other contexts and several explanations have been proposed for their occurrence. For example, Rochette *et al.* (1999), Potter & Stephenson (1988) and Borradaile & Puumala (1989) have proposed that inverse fabrics result from the presence of SD titanomagnetite grains within the rocks. Crystallization of secondary magnetic oxides in residual magma or as a result of hydrothermal alteration has also been evoked to be at the origin of ferromagnetic SD grain crystallization and therefore of inverse fabrics (Archanjo *et al.* 2002).

In the La Palisse basalt flow, the absence of SD grains is highlighted by hysteresis parameters and FORC diagrams, both indicating a large and homogenous grain size of ferromagnetic grains in the two sites and in all levels of the flow. Thus, the inverse magnetic fabrics cannot be explained by the presence of small SD

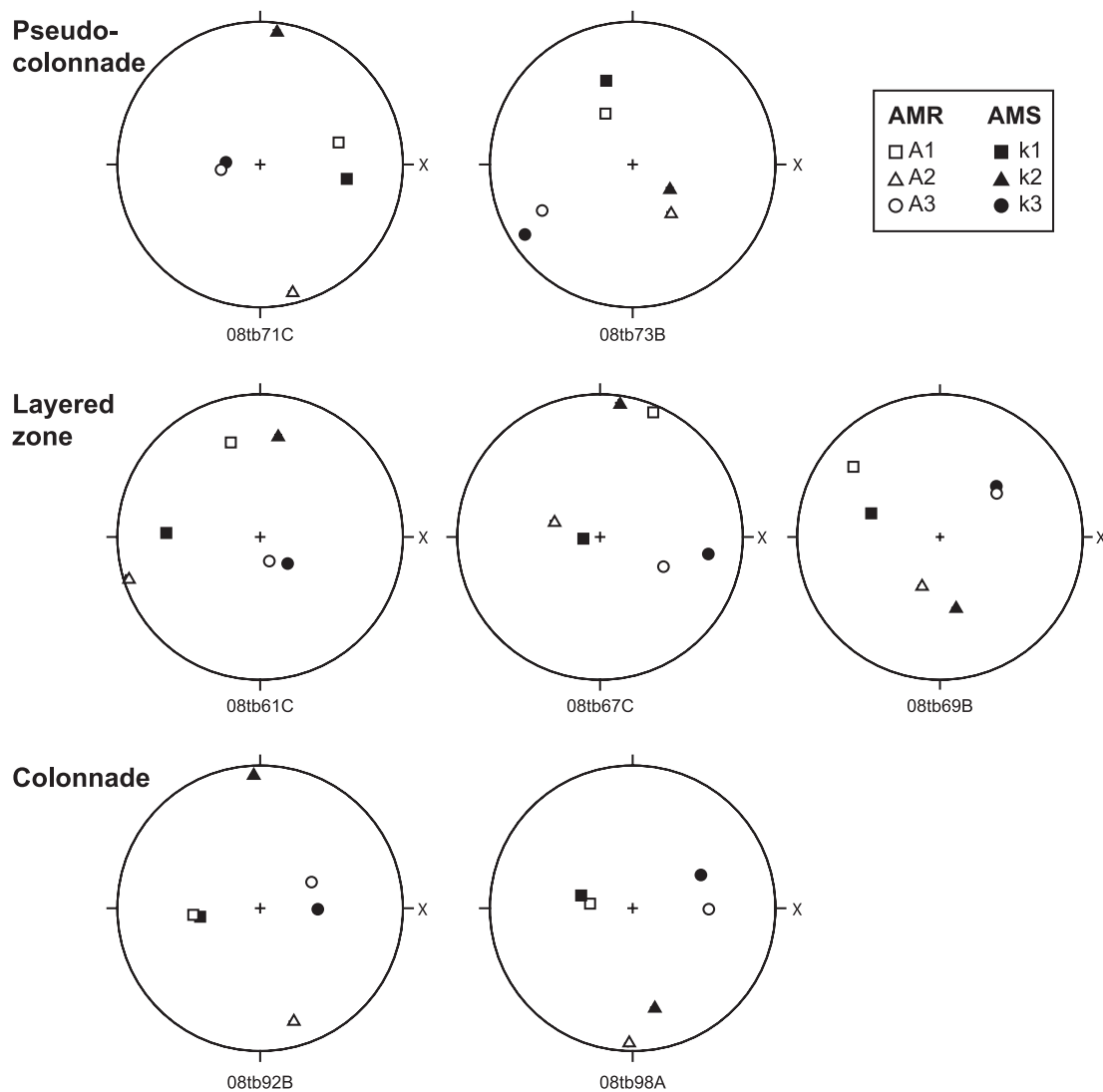


**Figure 12.** Principal directions of the AMS and ARM fabrics for samples from colonnade, layered zone and pseudo-colonnade, site 2 in the equal area, lower hemisphere projections in specimen coordinate system. The black and white symbols are AMS and ARM principal directions, respectively.

magnetic grains. The great homogeneity in size and shape of the titanomagnetite grains also excludes crystallization of secondary oxides during hydrothermal alteration processes. In addition, electron microprobe and thermomagnetic curves indicate that Ti-rich titanomagnetite grains, which are the main carrier of AMS, are relatively homogeneous in composition in the whole lava flow. The magnetic mineralogy study of the La Palisse basaltic lavas tends to exclude the presence of SD ferromagnetic grains as the cause of the inverse fabric. However, as underlined by Chadima *et al.* (2009), several studies have shown obvious inverse fabric in dykes whereas the magnetic grain size study from hysteresis measurements did not reveal SD grains evidences (e.g. Callot *et al.* 2001; DeFrates *et al.* 2006). Chadima *et al.* (2009) proposed to measure the anisotropy of remanent magnetization (ARM) when the presence of SD grains is supposed. In case of inverse AMS fabric, ARM shows a permutation of AMS maximum and minimum directions. In order to check the presence of these SD grains in the La Palisse samples, ARM measurements were performed (Fig. 12). ARM fabrics of the studied samples are characterized by  $K_3$  parallel to  $A_3$  (minimum axis of ARM) and therefore indicate no permutation between ARM

and AMS fabrics. These results confirm that inverse AMS fabric is not a consequence of SD grain occurrence.

Petrological and chemical study of the La Palisse basaltic lava flow (Boiron 2011) does not show significant difference in composition between samples of sites 1 and 2. Thermomagnetic data confirm that the samples are very fresh, unaffected by post-emplacment alteration processes. Magnetic susceptibility is high but relatively similar for both sites, in particular for the colonnade ( $4.9 \times 10^{-2}$  SI  $< K_m < 6.1 \times 10^{-2}$  SI). This point is important because a higher value of susceptibility to one of the sites could be associated with an increase of magnetic interactions due to a higher clustering of ferromagnetic grains, which could generate abnormal magnetic fabric (Fanjat *et al.* 2012). Various numerical and analogical modelling (Merle 1998; Cañón-Tapia & Pinkerton 2000; Cañón-Tapia & Chávez-Álvarez 2004) show that the shear intensity could impact on magnetic fabrics. When the shear is important, the foliation development promotes an orientation of the minimum axis  $K_3$  perpendicular to the shear plane. On the contrary, in the case of weaker shear intensity, the magnetic fabric is preferentially lineated and the maximum axis  $K_1$  tends to be perpendicular to the

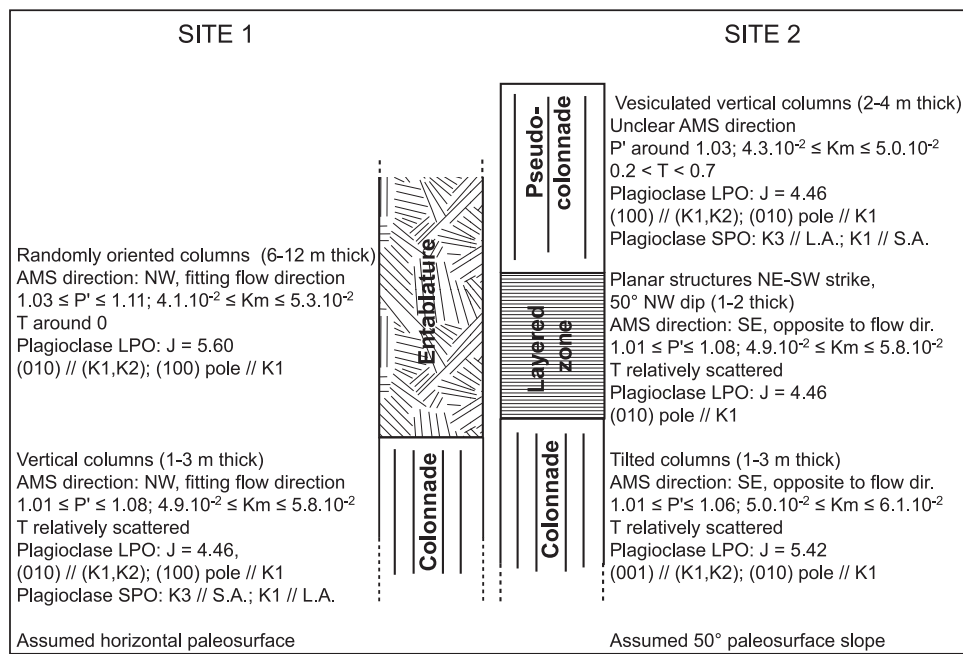


**Figure 13.** Summarize of site 1 and 2 characteristics (paleosurface slope, columns shape, AMS direction, magnetic properties, lattice-preferred orientation of plagioclase and the relationship between magnetic and crystallographic fabric). For plagioclase SPO, S.A. indicates the short axis and L.A. is the long axis.

shear plane. Elongation ration of the particles could also affect the orientations. It is particularly difficult to quantify in natural lava. However, images analysis from digital photos on thin sections does not show significant differences in grain size of minerals coming from similar areas (e.g. the top of the colonnade). In addition, neither the crystallographic fabric strength ( $J_{\text{index}}$ ) of plagioclase, nor the magnetic anisotropy values ( $P'$ ) do not show strong variations between the both sites that suggests relatively comparable amount of shearing strain during the latest stages of the lava flow evolution.

A synthesis of data characterizing the studied sites of the La Palisse lava flow is presented in Fig. 13. It clearly appears that the main difference between the both sites concerns the paleosurface slope, very gentle for site 1 and steep ( $50^\circ$ ) slope for site 2. C  n  n-Tapia *et al.* (1995, 1996, 1997) indicate that the morphology of a lava flow is strongly controlled by the rheology and the slope of the pre-existing terrain. The maximum of susceptibility axes are more scattered and sometimes even perpendicular to the flow direction when the slope of paleosurface is very weak whereas less scattered maximum axes are observed with a stronger slope. Numerical modelling of Merle (1998) shows that flowing over an inclined base produces complex stretch and flattening plane trajectories in the vertical plane and thus, generate significant gap between the stretching direction and the flow direction (and the associated fabric development).

Finally, the viscosity of the lava during emplacement can also have a great influence on the degree of anisotropy as shown by Hrouda *et al.* (2005). Such geological causes could explain the colonnade and the layered zone inverse fabrics of site 2.

## 8 CONCLUSIONS

In this AMS study, we show that the determination of the flow direction and the sense can be achieved through the use of the magnetic foliation imbrication, in particular at the base of the flow. Contrary to other studies that base the AMS analysis on the  $K_1$  directions

(with or without imbrication), the measurements on the La Palisse lava flow highlight the poor reliability of magnetic lineation. This can easily induce inversion between  $K_1$  and  $K_2$  during the flow.

EBSD data show clear correlations between plagioclase and clinopyroxene LPO: (100) plagioclase tends to be parallel to (001) clinopyroxene and (010) plagioclase tends to be parallel to (100) clinopyroxene. In addition, LPO orientations, and also shape-preferred orientations of plagioclase show tight relationship with principal AMS directions. For site 1, (010) plagioclase is parallel to the magnetic foliation ( $K_1$ ,  $K_2$ ) and coincides to the flow plane, and the pole of (100) plagioclase is parallel to  $K_1$  and coincides to the flow indicated by the preferred alignment of plagioclase laths. These close relationships between crystallographic and magnetic fabrics suggest a control of the silicate framework (plagioclase and clinopyroxene) on AMS carried by the titanomagnetite grains.

For both sampling sites (sites 1 and 2), the flow direction deduced from AMS is consistent with field evidences. However, only AMS in site 1 allows determining the geological flow sense. For site 2, the flow sense is systematically opposed to the geological flow sense. Relations between AMS and LPO are systematically different of those of site 1; for site 2, the pole of (010) plagioclase is always parallel to  $K_1$  for the three levels, the pole of (100) plagioclase is parallel to  $K_3$  for pseudo-colonnade, (001) plagioclase tends to be parallel to the magnetic foliation ( $K_1$ ,  $K_2$ ) for colonnade whereas the layered zone do not indicate other clear relations.

Petrographic observation, thermomagnetic curves as well as hysteresis parameters indicate that magnetic minerals are mainly sub-hedral Ti-rich titanomagnetite grains belonging to MD and PSD. FORC diagrams exclude a grain size population dominated by SD grain in the samples. Therefore, the permutation between  $K_1$  and  $K_3$  axes cannot be related to the presence of SD grains that is confirmed by ARM data.

Magnetic susceptibility parameters ( $P'$  and  $K_m$ ) are relatively similar for the two sites, except in the entablature of site 1 where the anisotropy degree ( $P'$ ) is higher than in the other levels. We also



observe that the layered zone (site 2) is not the equivalent of the entablature (site 1), although both are located in the middle part of the flow. The crystallographic fabric strength ( $J_{\text{index}}$ ) of plagioclase (and clinopyroxene) is also relatively similar in the two sites.

The main difference between site 1 and site 2 concerns the palaeosurface slope, very gentle for site 1 and steep ( $50^\circ$ ) slope for site 2 as indicated by the layered zone inclination and the tilt of the columns. Inverse fabrics of site 2 may be then due to other factors than magnetic grain size such as lava viscosity or the palaeosurface slope during the emplacement of the flow. However, additional analyses are needed to determine precisely which of these factors exerted the main control on the permutation of AMS axes.

If AMS appears as an efficient tool to reveal the structure of basalt flows and to deduce the flow direction, our study supports that inverse magnetic fabrics can occur even in the absence of SD grains. Recently, Chadima *et al.* (2009) proposed to use preferably ARM rather than AMS fabric to determine flow direction and tectonic interpretations of magnetic fabric in dykes. However, this technique remains less usual than the measurement of AMS, which has become a common tool in rock magnetism. In lava flows, AMS measurements coupled with local analyses such as LPO obtained through EBSD technique or SPO deduced from image analysis could allow preventing misinterpretations based on AMS fabrics alone.

## ACKNOWLEDGEMENTS

The authors thank C. Cortial from the 'Groupe géologique de la Haute-Loire' for his participation in the field prospection and B. Aneesa Lehman (Department of Geology, Southern Illinois University) for the hysteresis measurements. G. Hoareau and two anonymous reviewers are gratefully acknowledged for their valuable comments and remarks that have helped improving this paper.

## REFERENCES

- Archanjo, C., Araujo, M. & Launeau, P., 2002. Fabric of the Rio Ceará—Mirim mafic dike swarm (northeastern Brazil) determined by anisotropy of magnetic susceptibility and image analysis, *J. geophys. Res.*, **107**(B3), 2046.
- Aubele, J.C., Crumpler, L. & Elston, W.E., 1988. Vesicle zonation and vertical structure of basalt flows, *J. Volc. Geotherm. Res.*, **35**(4), 349–374.
- Bascou, J., Camps, P. & Dautria, J., 2005. Magnetic versus crystallographic fabrics in a basaltic lava flow, *J. Volc. Geotherm. Res.*, **145**(1–2), 119–135.
- Bertolo, S., Nimis, P. & Dal Negro, A., 1994. Low-Ca augite from experimental alkali basalt at 18 kbar; structural variation near the miscibility gap, *Am. Miner.*, **79**(7–8), 668–674.
- Boiron, T., 2011. Étude multi-échelle des variations structurales, géochimiques et des propriétés magnétiques des coulées basaltiques prismées: exemple de la coulée La Palisse (Ardèche) et de Saint-Arcons-d'Allier (Haute-Loire), *PhD thesis*, École nationale supérieure des mines, Saint-Etienne, pp. 279.
- Borradaile, G.J. & Puumala, M., 1989. Synthetic magnetic fabrics in a plasticine medium, *Tectonophysics*, **164**(1), 73–78.
- Borradaile, G.J. & Henry, B., 1997. Tectonic applications of magnetic susceptibility and its anisotropy, *Earth-Sci. Rev.*, **42**(1–2), 49–93.
- Borradaile, G.J. & Jackson, M., 2004. Anisotropy of magnetic susceptibility (AMS), magnetic petrofabrics of deformed rocks, in *Magnetic Fabrics*, Vol. 238, pp. 299–360, eds Martín-Hernández, F., Lünenburg, C.M., Aubourg, C. & Jackson, M., Geological Society of London, Special Publication.
- Bouchez, J.-L., 2000. Anisotropie de susceptibilité magnétique et fabrique des granites, *Comp. Ren. l'Acad. Sci.—Ser. IIA—Earth planet. Sci.*, **330**(1), 1–14.
- Bunge, H.J., 1982. *Texture Analysis in Materials Science*, Butterworths, London, 593 pp.
- Callot, J.P., Geoffroy, L., Aubourg, C., Pozzi, J.P. & Mege, D., 2001. Magma flow directions of shallow dykes from the East Greenland volcanic margin inferred from magnetic fabric studies, *Tectonophysics*, **335**(3–4), 313–329.
- Callot, J.P. & Guichet, X., 2003. Rock texture and magnetic lineation in dykes: a simple analytical model, *Tectonophysics*, **366**(3–4), 207–222.
- Cánón-Tapia, E., Walker, G.P.L. & Herrero-Bervera, E., 1995. Magnetic fabric and flow direction in basaltic pahoehoe lava of Xitle Volcano, Mexico, *J. Volc. Geotherm. Res.*, **65**, 249–263.
- Cánón-Tapia, E., Walker, G.P.L. & Herrero-Bervera, E., 1996. The internal structure of lava flows—insights from AMS measurements. 1. Near-vent 'a', *J. Volc. Geotherm. Res.*, **70**(1–2), 21–36.
- Cánón-Tapia, E., Walker, G.P.L. & Herrero-Bervera, E., 1997. The internal structure of lava flows—insights from AMS measurements. 2. Hawaiian pahoehoe, toothpaste lava and 'a'(a)over-bar, *J. Volc. Geotherm. Res.*, **76**(1–2), 19–46.
- Cañón-Tapia, E. & Pinkerton, H., 2000. The anisotropy of magnetic susceptibility of lava flows: an experimental approach, *J. Volc. Geotherm. Res.*, **98**(1–4), 219–233.
- Cañón-Tapia, E., 2004. Anisotropy of magnetic susceptibility of lava flows and dykes: a historical account, *Geol. Soc., Lond., Spec. Publ.*, **238**(1), 205–225.
- Cañón-Tapia, E. & Chávez-Álvarez, M., 2004. Theoretical aspects of particle movement in flowing magma: implication for the anisotropy of magnetic susceptibility of dykes and lava flows, *Geol. Soc., Lond., Spec. Publ.*, **238**(1), 227–249.
- Chadima, M., Cajz, V. & Týcová, P., 2009. On the interpretation of normal and inverse magnetic fabric in dikes: examples from the Eger Graben, NW Bohemian Massif, *Tectonophysics*, **466**(1–2), 47–63.
- Day, R., Fuller, M. & Schmidt, V.A., 1977. Hysteresis properties of titanomagnetites: grain-size and compositional dependence, *Phys. Earth planet. Inter.*, **13**(4), 260–267.
- DeFrates, J., Malone, D. & Craddock, J., 2006. Anisotropy of magnetic susceptibility (AMS) analysis of basalt dikes at Cathedral Cliffs, WY: implications for Heart Mountain faulting, *J. Struct. Geol.*, **28**(1), 9–18.
- Dragoni, M., Lanza, R. & Tallarico, A., 1997. Magnetic anisotropy produced by magma flow: theoretical model and experimental data from Ferrar dolerite sills (Antarctica), *Geophys. J. Int.*, **128**(1), 230–240.
- Dunlop, D.J. & Özdemir, Ö., 1997. *Rock Magnetism: Fundamentals and Frontiers*, Cambridge University Press, New York, 573 pp.
- Dunlop, D.J., 2002. Theory and application of the Day plot (Mrs/Ms versus Hcr/Hc)1. Theoretical curves and tests using titanomagnetite data, *J. geophys. Res.*, **107**(B3), 2057.
- Fanjat, G., Camps, P., Shcherbakov, V., Barou, F., Sougrati, M.T. & Perrin, M., 2012. Magnetic interactions at the origin of abnormal magnetic fabrics in lava flows: a case study from Kerguelen flood basalts, *Geophys. J. Int.*, doi:10.1111/j.1365-246X.2012.05421.x.
- Ferré, E.C. & Ameglio, L., 2000. Preserved magnetic fabrics vs. annealed microstructures in the syntectonic recrystallised George granite, South Africa, *J. Struct. Geol.*, **22**(8), 1199–1219.
- Ferré, E.C., 2002. Theoretical models of intermediate and inverse AMS fabrics, *Geophys. Res. Lett.*, **29**(7), 1127.
- Ferré, E.C., Teyssier, C., Jackson, M., Thill, J.W. & Rainey, E.S.G., 2003. Magnetic susceptibility anisotropy: a new petrofabric tool in migmatites, *J. geophys. Res.*, **108**(B2), 2086.
- Geoffroy, L., Callot, J.P., Aubourg, C. & Moreira, M., 2002. Magnetic and plagioclase linear fabric discrepancy in dykes: a new way to define the flow vector using magnetic foliation, *Terra Nova*, **14**(3), 183–190.
- Gil-Imaz, A., Pocovi, A., Lago, M., Gale, C., Arranz, E., Rillo, C. & Guerrero, E., 2006. Magma flow and thermal contraction fabric in tabular intrusions inferred from AMS analysis. A case study in a late-Variscan folded sill of the Albarracín Massif (southeastern Iberian Chain, Spain), *J. Struct. Geol.*, **28**, 641–653.
- Grégoire, V., de Saint Blanquet, M., Nédélec, A. & Bouchez, J.L., 1995. Shape anisotropy versus magnetic interactions of magnetite grains:

- experiments and application to AMS in granitic rocks, *Geophys. Res. Lett.*, **22**(20), 2765–2768.
- Guérin, G. & Gillot, P., 2007. Nouveaux éléments de chronologie du volcanisme Pléistocène du bas Vivarais (Ardèche, France) par thermoluminescence, *C. R. Geosci.*, **339**(1), 40–49.
- Hargraves, R.B., Johnson, D. & Chan, C.Y., 1991. Distribution anisotropy: the cause of AMS in igneous rocks? *Geophys. Res. Lett.*, **18**(12), 2193–2196.
- Hartstra, R., 1982. Grain-size dependence of initial susceptibility and saturation magnetization-related parameters of 4 natural magnetites in the PSD-MD range, *Geophys. J. R. astr. Soc.*, **71**(2), 477–495.
- Hastie, W.W., Watkeys, M.K. & Aubourg, C., 2011. Significance of magnetic and petrofabric in Karoo-feeder dykes, northern Lebombo, *Tectonophysics*, **513**(1–4), 96–111.
- Henry, B., Jordanova, D., Jordanova, N., Souque, C. & Robion, P., 2003a. Anisotropy of magnetic susceptibility of heated rocks, *Tectonophysics*, **366**(3–4), 241–258.
- Henry, B., Plenier, G. & Camps, P., 2003b. Post-emplacement tilting of lava flows inferred from magnetic fabric study: the example of oligocene lavas in the Jeanne d'Arc Peninsula (Kerguelen islands), *J. Volc. Geotherm. Res.*, **127**(1–2), 153–164.
- Herrero-Bervera, E., Walker, G.P.L., Cañón-Tapia, E. & Garcia, M.O., 2001. Magnetic fabric and inferred flow direction of dikes, coneshells and sill swarms, Isle of Skye, Scotland, *J. Volc. Geotherm. Res.*, **106**(3–4), 195–210.
- Hrouda, F., 1992. Separation of a component of tectonic deformation from a complex magnetic fabric, *J. Struct. Geol.*, **14**(1), 65–71.
- Hrouda, F., Chlupacova, M., Schulmann, K., Smid, J. & Zavada, P., 2005. On the effect of lava viscosity on the magnetic fabric intensity in alkaline volcanic rocks, *Stud. Geophys. Geod.*, **49**(2), 191–212.
- Jelinek, V., 1978. Statistical processing of anisotropy of magnetic susceptibility measured on groups of specimens, *Stud. Geophys. Geod.*, **22**(1), 50–62.
- Jelinek, V., 1981. Characterization of the magnetic fabric of rock, *Tectonophysics*, **79**(3–4), 63–67.
- Knight, M.D. & Walker, G.P.L., 1988. Magma flow directions in dikes of the Koolau complex, Oahu, determined from magnetic fabric studies, *J. geophys. Res.*, **93**(B5), 4301–4319.
- Lattard, D., Engelmann, R., Kontny, A. & Sauerzapf, U., 2006. Curie temperatures of synthetic titanomagnetites in the Fe-Ti-O system: effects of composition, crystal chemistry, and thermomagnetic methods, *J. geophys. Res.-Solid Earth*, **111**(B12), S28.
- Launeau, P. & Robin, P.-Y.F., 1996. Fabric analysis using the intercept method, *Tectonophysics*, **267**(1–4), 91–119.
- Launeau, P. & Robin, P.-Y.F., 2005. Determination of fabric and strain ellipsoids from measured sectional ellipses—implementation and applications, *J. Struct. Geol.*, **27**, 2223–2233.
- Launeau, P., Archanjo, C.J., Picard, D., Arbaret, L. & Robin, P.-Y.F., 2010. Two- and three-dimensional shape fabric analysis by the intercept method in grey levels, *Tectonophysics*, **492**, 230–239.
- Lebas, M.J., Lemaitre, R.W., Streckeisen, A. & Zanettin, B., 1986. A chemical classification of volcanic rocks based on the total alkali-silica diagram, *J. Petrol.*, **27**(3), 745–750.
- Long, P.E. & Wood, B.J., 1986. Structures, textures, and cooling histories of Columbia river Basalt flows, *Geol. Soc. Am. Bull.*, **97**(9), 1144–1155.
- Loock, S., Diot, H., Van Wyk de Vries, B., Launeau, P., Merle, O., Vadeboin, F. & Petronis, M.S., 2008. Lava flow internal structure found from AMS and textural data: an example in methodology from the Chaîne des Puys, France, *J. Volc. Geotherm. Res.*, **177**(4), 1092–1104.
- Merle, O., 1998. Internal strain within lava flows from analogue modelling, *J. Volc. Geotherm. Res.*, **81**(3–4), 189–206.
- O'Donovan, J., Facey, D. & O'Reilly, W., 1986. The magnetization process in titanomagnetite (Fe<sub>2.4</sub>Ti<sub>0.6</sub>O<sub>4</sub>) in the 1–30 µm particle size range, *Geophys. J. R. astr. Soc.*, **87**(3), 897–916.
- Park, J.K., Tanczyk, E.I. & Desbarats, A., 1988. Magnetic fabric and its significance in the 1400 Ma Mealy Diabase Dykes of Labrador, Canada, *J. Geophys. Res.*, **93**(B11), 13 673–13 687.
- Petronis, M. & Geissman, J., 2009. Anisotropy of magnetic susceptibility data bearing on the transport of mid-tertiary regional ignimbrites, Candelaria Hills area, West-Central Nevada, *Bull. Volc.*, **71**, 121–151.
- Pike, C., Roberts, A. & Verosub, K., 1999. Characterizing interactions in fine magnetic particle systems using first order reversal curves, *J. appl. Phys.*, **85**(9), 6660–6667.
- Plenier, G., Camps, P., Henry, B. & Ildefonse, B., 2005. Determination of flow directions by combining AMS and thin-section analyses: implications for Oligocene volcanism in the Kerguelen Archipelago (southern Indian Ocean), *Geophys. J. Int.*, **160**(1), 63–78.
- Potter, D.K. & Stephenson, A., 1988. Single-domain particles in rocks and magnetic fabric analysis, *Geophys. Res. Lett.*, **15**(10), 1097–1100.
- Raposo, M. & Berquo, T., 2008. Tectonic fabric revealed by AARM of the proterozoic mafic dike swarm in the Salvador city (Bahia state): Sao Francisco Craton, NE Brazil, *Phys. Earth planet. Inter.*, **167**(3–4), 179–194.
- Roberts, A.P., Pike, C.R. & Verosub, K.L., 2000. First-order reversal curve diagrams: a new tool for characterizing the magnetic properties of natural samples, *J. geophys. Res.*, **105**(B12), doi:10.1029/2000JB900326.
- Rochette, P., Jackson, M. & Aubourg, C., 1992. Rock magnetism and the interpretation of anisotropy of magnetic susceptibility, *Rev. Geophys.*, **30**(3), 209–226.
- Rochette, P., Aubourg, C. & Perrin, M., 1999. Is this magnetic fabric normal? A review and case studies in volcanic formations, *Tectonophysics*, **307**(1–2), 219–234.
- Smith, J.V., 2002. Structural analysis of flow-related textures in lavas, *Earth-Sci. Rev.*, **57**, 279–297.
- Staudigel, H., Gee, J., Tauxe, L. & Varag, R.J., 1992. Shallow intrusive directions of sheeted dikes in the Troodos ophiolite: anisotropy of magnetic susceptibility and structural data, *Geology*, **20**(9), 841–844.
- Tarling, D.H. & Hrouda, F., 1993. *The Magnetic Anisotropy of Rocks*, Chapman and Hall, London, 217 pp.
- Ventura, G., De Rosa, R., Colleta, E. & Mazzuoli, R., 1996. Deformation patterns in a high-viscosity lava flow inferred from the crystal preferred orientation and imbrication structures: an example from Salina (Aeolian Islands, southern Tyrrhenian Sea, Italy), *Bull. Volc.*, **57**, 555–562.
- Wechsler, B.A., Lindsley, D.H. & Prewitt, C.T., 1984. Crystal structure and cation distribution in titanomagnetites (Fe (sub 3-x) Ti x O<sub>4</sub>), *Am. Miner.*, **69**(7–8), 754–770.
- Wenk, H.R., Lindsley, D. & Prewitt, C.T., 1980. The average structure of An 62–66 labradorite, *Am. Miner.*, **65**(1–2), 81–95.
- Zhu, R., Shi, C. & Liu, Q., 2003. Anisotropy of magnetic susceptibility of Hannuoba basalt, northern China: constrain on the vent position of the lava sequences, *Geophys. Res. Lett.*, **30**(2), 1066.